

Fundamental Equations of State for Parahydrogen, Normal Hydrogen, and Orthohydrogen

J. W. Leachman^{a)}

Center for Applied Thermodynamic Studies (CATS), University of Idaho, Moscow, Idaho 83844, USA

R. T Jacobsen

College of Engineering, Idaho State University, Pocatello, Idaho 83209, USA

S. G. Penoncello

Center for Applied Thermodynamics Studies (CATS), University of Idaho, Moscow, Idaho 83844, USA

E. W. Lemmon^{b)}

Thermophysical Properties Division, National Institute of Standards and Technology, 325 Broadway, Boulder, Colorado 80305, USA

(Received 15 January 2009; accepted 9 June 2009; published online 4 September 2009)

If the potential for a boom in the global hydrogen economy is realized, there will be an increase in the need for accurate hydrogen thermodynamic property standards. Based on current and anticipated needs, new fundamental equations of state for parahydrogen, normal hydrogen, and orthohydrogen were developed to replace the existing property models. To accurately predict thermophysical properties near the critical region and in liquid states, the quantum law of corresponding states was applied to improve the normal hydrogen and orthohydrogen formulations in the absence of available experimental data. All three equations of state have the same maximum pressure of 2000 MPa and upper temperature limit of 1000 K. Uncertainty estimates in this paper can be considered to be estimates of a combined expanded uncertainty with a coverage factor of 2 for primary data sets. The uncertainty in density is 0.04% in the region between 250 and 450 K and at pressures up to 300 MPa. The uncertainties of vapor pressures and saturated liquid densities vary from 0.1% to 0.2%. Heat capacities are generally estimated to be accurate to within 1%, while speed-of-sound values are accurate to within 0.5% below 100 MPa. © 2009 by the U.S. Secretary of Commerce on behalf of the United States. All rights reserved. [doi:10.1063/1.3160306]

Key words: density; equation of state; heat capacity; hydrogen; normal hydrogen; orthohydrogen; parahydrogen; thermodynamic properties; vapor pressure.

CONTENTS

1. Nomenclature.	724	5.2. Ideal-Gas Contributions to the Reduced Helmholtz Free Energy.	730
2. Introduction.	724	5.3. Residual Contribution to the Reduced Helmholtz Free Energy.	731
3. Normal Hydrogen: A 3:1 Mixture of Orthohydrogen and Parahydrogen.	724	5.4. Fixed-Point Properties.	732
4. The Quantum Law of Corresponding States.	726	5.5. Vapor Pressures.	733
5. Equations of State and Ancillary Equations.	728	6. Comparison of Calculated Data to Experimental Data.	734
5.1. The Regression Process.	729	6.1. Comparison of Calculated Parahydrogen Data to Experimental Data.	734
		6.2. Comparison of Data Predicted Using the Quantum Law of Corresponding States.	737
		6.3. Comparison of Calculated Normal Hydrogen Data to Experimental Data.	738
		6.4. Comparison of Calculated Orthohydrogen Data to Transformed Experimental Data.	741

^{a)}Present address: Cryogenics Laboratory, University of Wisconsin-Madison, 1500 Engineering Hall Drive, Rm. 1335, Madison, Wisconsin 53706, USA.

^{b)}Author to whom correspondence should be addressed. Electronic mail: eric.lemmon@nist.gov

© 2009 by the U.S. Secretary of Commerce on behalf of the United States. All rights reserved.

7.	Results and Recommendations for Future Research.....	743
8.	Acknowledgments.....	747
9.	Appendix.....	747
10.	References.....	747

List of Tables

1.	Critical-point and triple-point properties for normal hydrogen and parahydrogen used in the EOS formulations of Younglove ⁷	725
2.	Values of the quantum parameter for several fluids ¹⁹	726
3.	Parameters and coefficients of the parahydrogen, normal hydrogen, and orthohydrogen ideal-gas heat capacity equations, Eq. (25).....	728
4.	Parameters and coefficients of the parahydrogen, normal hydrogen, and orthohydrogen ideal-gas Helmholtz free energy equations, Eq. (31).....	729
5.	Parameters and coefficients of the new parahydrogen, normal hydrogen, and orthohydrogen equations of state.....	730
6.	Parameters of the Gaussian terms in the new parahydrogen, normal hydrogen, and orthohydrogen equations of state.....	730
7.	Critical- and triple-point properties used by the new parahydrogen, normal hydrogen, and orthohydrogen equations of state (this work)...	731
8.	Parameters and coefficients of the parahydrogen, normal hydrogen, and orthohydrogen vapor pressure ancillary equations, Eq. (33).....	732
9.	Parahydrogen experimental data sets and AAD from the new and Younglove ⁷ equations of state.....	732
10.	Calculated parahydrogen vapor-pressure data (this work) and the data transformed to the normal hydrogen and orthohydrogen surfaces of state.....	737
11.	Selected parahydrogen single-phase density data and the data transformed to the normal hydrogen and orthohydrogen surfaces of state..	738
12.	Normal hydrogen experimental data and AAD from the new and Younglove ⁷ EOS.....	739
13.	Tabulated thermodynamic properties of parahydrogen at saturation.....	745
14.	Tabulated thermodynamic properties of normal hydrogen at saturation.....	746
15.	Tabulated thermodynamic properties of orthohydrogen at saturation.....	746

List of Figures

1.	Calculated ideal-gas heat capacities of parahydrogen, normal hydrogen, and
----	--

orthoxygen.....	725	
2.	Calculated vapor-pressure differences between liquid normal hydrogen and parahydrogen.....	726
3.	Reduced temperature versus quantum parameter.....	727
4.	Reduced pressure versus quantum parameter....	727
5.	Comparison of calculated ideal-gas isobaric heat capacities for parahydrogen to literature data.....	728
6.	Comparison of calculated ideal-gas isobaric heat capacities for normal hydrogen to literature data.....	729
7.	Comparison of calculated ideal-gas isobaric heat capacities for orthohydrogen to literature data.....	729
8.	Predicted pressures versus densities at extreme conditions for the new parahydrogen EOS.....	731
9.	Comparison of calculated second virial coefficients plotted versus temperature for the new parahydrogen EOS (top) and the parahydrogen EOS of Younglove (bottom) to experimental data.....	733
10.	Comparison of calculated third virial coefficients plotted versus temperature for the new parahydrogen EOS (top) and the parahydrogen EOS of Younglove (bottom) to experimental data.....	733
11.	Comparison of calculated saturation heat capacities for the new parahydrogen EOS (top) and the parahydrogen EOS of Younglove (bottom) to experimental data.....	733
12.	Comparison of calculated isochoric heat capacities for the new parahydrogen EOS (top) and the parahydrogen EOS of Younglove (bottom) to experimental data.....	733
13.	Comparison of calculated isobaric heat capacities for the new parahydrogen EOS (top) and the parahydrogen EOS of Younglove (bottom) to experimental data.....	734
14.	Comparison of calculated vapor pressures for the new parahydrogen EOS (top) and the parahydrogen EOS of Younglove (bottom) to experimental data.....	734
15.	Comparison of calculated sound speeds for the new parahydrogen EOS (top) and the parahydrogen EOS of Younglove (bottom) to experimental data.....	734
16.	Comparison of calculated densities for the new parahydrogen EOS (left) and the parahydrogen EOS of Younglove (right) to experimental data (data displayed in 10 K increments from 10 to 70 K).....	735
17.	Comparison of calculated densities for the new parahydrogen EOS (left) and the parahydrogen EOS of Younglove (right) to experimental data (data displayed in 10 K increments from 70 to 140 K).....	735

- | | | | | | |
|-----|--|-----|-----|--|-----|
| 18. | Comparison of calculated densities for the new parahydrogen EOS (left) and the parahydrogen EOS of Younglove (right) to experimental data (data displayed in 10 K increments from 150 to 250 K)..... | 736 | 31. | Comparison of calculated densities plotted versus pressure for the new normal hydrogen EOS (left) and the normal hydrogen EOS of Younglove (right) to experimental data (data plotted in 10 K increments from 70 to 140 K).. | 742 |
| 19. | Comparison of calculated densities for the new parahydrogen EOS (left) and the parahydrogen EOS of Younglove (right) to experimental data (data displayed in 10 K increments from 270 to 360 K)..... | 736 | 32. | Comparison of calculated densities plotted versus pressure for the new normal hydrogen EOS (left) and the normal hydrogen EOS of Younglove (right) to experimental data (data plotted in 10 K increments from 150 to 250 K)..... | 742 |
| 20. | Comparison of calculated densities for the new parahydrogen EOS (left) and the parahydrogen EOS of Younglove (right) to experimental data (data displayed in listed increments from 370 to 580 K)..... | 736 | 33. | Comparison of calculated densities plotted versus pressure for the new normal hydrogen EOS (left) and the normal hydrogen EOS of Younglove (right) to experimental data (data plotted in 10 K increments from 270 to 360 K)..... | 742 |
| 21. | Comparison of calculated densities for the new parahydrogen EOS (left) and the parahydrogen EOS of Younglove (right) to experimental data (data displayed in 10 K increments from 670 to 880 K)..... | 736 | 34. | Comparison of calculated densities plotted versus pressure for the new normal hydrogen EOS (left) and the normal hydrogen EOS of Younglove (right) to experimental data (data plotted in listed increments from 370 to 580 K)..... | 743 |
| 22. | Comparison of calculated densities for the new parahydrogen EOS (top) and the parahydrogen EOS of Younglove (bottom) to experimental data (data plotted against pressure)..... | 737 | 35. | Comparison of calculated densities plotted versus pressure for the new normal hydrogen EOS (left) and the normal hydrogen EOS of Younglove (right) to experimental data (data plotted in listed increments from 670 to 880 K)..... | 743 |
| 23. | Comparison of calculated densities for the new parahydrogen EOS (top) and the parahydrogen EOS of Younglove (bottom) to experimental data (data plotted against temperature)..... | 737 | 36. | Comparison of calculated densities plotted versus pressure for the new normal hydrogen EOS (top) and the normal hydrogen EOS of Younglove (bottom) to experimental data..... | 743 |
| 24. | Comparison of calculated vapor pressures for the new normal hydrogen EOS to experimental and predicted data..... | 738 | 37. | Comparison of calculated densities plotted versus temperature for the new normal hydrogen EOS (top) and the normal hydrogen EOS of Younglove (bottom) to experimental data..... | 744 |
| 25. | Comparison of calculated densities for the new normal hydrogen EOS to experimental and predicted data..... | 738 | 38. | Comparison of calculated vapor pressures plotted versus temperature for the new orthohydrogen EOS to experimental and predicted data..... | 744 |
| 26. | Comparison of calculated second virial coefficients plotted versus temperature for the new normal hydrogen EOS (top) and the normal hydrogen EOS of Younglove (bottom) to experimental data..... | 741 | 39. | Comparison of calculated sound speeds plotted versus pressure for the new orthohydrogen EOS to predicted data..... | 744 |
| 27. | Comparison of calculated third virial coefficients plotted versus temperature for the new normal hydrogen EOS (top) and the normal hydrogen EOS of Younglove (bottom) to experimental data..... | 741 | 40. | Comparison of calculated densities plotted versus pressure for the new orthohydrogen EOS to experimental and predicted data (data shown in increments from 10 to 150 K)..... | 744 |
| 28. | Comparison of calculated vapor pressures plotted versus temperature for the new normal hydrogen EOS (top) and the normal hydrogen EOS of Younglove (bottom) to experimental data and transformed data..... | 741 | 41. | Comparison of calculated densities plotted versus pressure for the new orthohydrogen EOS to experimental and predicted data (data shown in increments from 150 to 350 K)..... | 745 |
| 29. | Comparison of calculated sound speeds plotted versus pressure for the new normal hydrogen EOS (top) and the normal hydrogen EOS of Younglove (bottom) to experimental data..... | 741 | 42. | Comparison of calculated densities plotted versus pressure for the new orthohydrogen EOS to experimental and predicted data (data | |
| 30. | Comparison of calculated densities plotted versus pressure for the new normal hydrogen EOS (left) and the normal hydrogen EOS of Younglove (right) to experimental data (data | | | | |

shown in increments from 350 to 880 K)..... 745

1. Nomenclature

a	= Helmholtz free energy, J/mol
B	= Second virial coefficient, cm ³ /mol
C	= Third virial coefficient, cm ⁶ /mol ²
c_p	= Isobaric heat capacity, J/(mol K)
c_v	= Isochoric heat capacity, J/(mol K)
h	= Enthalpy, J/mol
\hbar	= Reduced Planck's constant, J s
M	= Molar mass, g/mol
N_A	= Avogadro's number, mol ⁻¹
p	= Pressure, MPa
R	= Molar gas constant, 8.314 472 J/(mol K)
r	= Radius of interaction, m
S	= Sum of squares
s	= Entropy, J/(mol K)
T	= Temperature, K
U	= Intermolecular potential, J/mol
W	= Statistical weight
w	= Speed of sound, m/s
Z	= Compressibility factor
α	= Reduced Helmholtz energy
ε	= Fluid-specific parameter of the Lennard-Jones potential, J/mol
δ	= Reduced density
Λ	= Quantum parameter
ρ	= Molar density, mol/dm ³
σ	= Intermolecular distance for Lennard-Jones potential, m
τ	= Inverse reduced temperature
ψ	= Wave function

Subscripts

c	= Critical-point property
r	= Reduced property
ortho	= Orthohydrogen property
para	= Parahydrogen property
norm	= Normal hydrogen property
σ	= Saturation property
t	= Triple-point property
0	= Reference property

Superscripts

*	= Quantum reduced property
r	= Real-fluid property
0	= Ideal-gas property

2. Introduction

Two recently completed surveys of the thermophysical properties of hydrogen establish the need for new equations of state for the thermodynamic properties of the various forms of hydrogen and for new formulations for the transport properties viscosity and thermal conductivity.^{1,2} This paper describes new equations of state for parahydrogen and normal hydrogen that were developed to replace the existing

equations of state and an equation of state (EOS) that was developed for orthohydrogen. The quantum law of corresponding states (QLCS) was used to supplement experimental normal hydrogen thermophysical property data and was verified by comparison to experimental data. The QLCS allowed the new equation of state for orthohydrogen to be based on a transformation of the data used in the normal hydrogen and parahydrogen formulations. The creation of an orthohydrogen EOS is intended to supplement a hydrogen mixture model that is the topic of future research. Although the bulk of the work is presented in this publication, further details are given in the thesis of Leachman.³

The new parahydrogen, normal hydrogen, and orthohydrogen equations of state consist of 14 terms and use a form similar to the equation described by Lemmon and Jacobsen⁴ and Span *et al.*⁵ The equations of state are explicit in the Helmholtz free energy and are valid for temperatures from the triple-point temperatures [13.8033 K for parahydrogen,⁶ 13.957 K for normal hydrogen (this work), and 14.008 K for orthohydrogen (this work)] to 1000 K and for pressures up to 2000 MPa, and the extrapolation is well behaved at much higher temperatures and pressures. Comparisons to available experimental data are given that establish the accuracy of properties calculated using the equations of state.

The EOS for parahydrogen developed by Younglove⁷ was based on work during the 1970s through the early 1980s at the National Bureau of Standards (NBS), in Boulder, CO, now the National Institute of Standards and Technology (NIST). The Younglove⁷ equation was based on experimental data for the thermodynamic properties of pure parahydrogen and was modified to predict thermodynamic properties of normal hydrogen by replacing the ideal-gas heat capacity equation and fixed-point properties of the parahydrogen model with values for normal hydrogen. The resulting models by Younglove⁷ for the calculation of thermodynamic properties of normal hydrogen and parahydrogen use the International Practical Temperature Scale of 1968, and the upper limits in pressure and temperature of the equations of state are 121 MPa and 400 K. These models were used in previous versions of NIST's standard properties package, REFPROP.⁸

The differences in the surfaces of state for parahydrogen, normal hydrogen, and orthohydrogen can be explained through quantum mechanics. Before the new equations of state are discussed, it is necessary to describe the differences in the parahydrogen and orthohydrogen molecules, because the molecular differences determine the differences observed in the experimental data and the differences in the new equations of state.

3. Normal Hydrogen: A 3:1 Mixture of Orthohydrogen and Parahydrogen

Bonhoeffer and Harteck,⁹ about the same time as Eucken and Hiller,¹⁰ were able to observe changes in property values of samples of hydrogen held at low temperatures for several hours. Because the samples were nearly isolated, the only

possible cause for the change was a conversion of the molecules from one spin state to another spin state possessing different property values. This observation came as no surprise, as Heisenberg and Hund had explained with quantum theory the existence of two different spin states for helium, orthohelium and parahelium and postulated a similar occurrence for hydrogen.^{11,12} Bonhoeffer and Harteck^{9,12} chose the names orthohydrogen and parahydrogen for the different forms, similar to the nomenclature chosen by Heisenberg for the helium molecule. Heisenberg chose “ortho,” meaning straight, right, and proper, from the Greek prefix (orthos), to represent the dominant concentration at room temperature. He chose the prefix “para,” meaning abnormal, to describe the form prevalent at low temperatures. The differentiating feature of the two forms is the relative orientation of the nuclear spin of the individual atoms. The cause of the difference in spins is the parity in the structure of the hydrogen molecule.

It is well established from particle physics that electrons and protons have a magnetic quantum number or spin of $\frac{1}{2}$ and an antisymmetric Schrödinger wave function. There is only one particle, the proton, present in each of the two nuclei in a hydrogen molecule. Fundamental particles having a spin of $\frac{1}{2}$ are indistinguishable from each other and are classified as fermions. Applying quantum mechanical addition, when the spins are antisymmetric they cancel each other and the net spin is 0; when they are symmetric the net spin is 1. The significance of this becomes apparent when the vibrational, rotational, and nuclear spin wave functions are combined into the total nuclear wave function for the molecule:

$$\psi_{\text{tot}} = \psi_{\text{vib}}\psi_{\text{rot}}\psi_{\text{spin}} \quad (1)$$

The vibrational contribution is always symmetric due to the linear-diatomic nature of the molecule and the lack of particle exchange between nuclei.¹³ Combining the one possible state of the vibration contribution, the two possible states of the nuclear spin, and the requirement that the total nuclear wave function be antisymmetric, two possible cases arise:

$$(\text{antisym}) = (\text{sym})(\text{sym})(\text{antisym}), \quad (2)$$

$$(\text{antisym}) = (\text{sym})(\text{antisym})(\text{sym}). \quad (3)$$

Thus, the total wave function of these is antisymmetric, as shown in Eqs. (2) and (3). The rotational wave function (ψ_{rot}) is symmetric in Eq. (2) and antisymmetric in Eq. (3). The question remains whether the symmetric rotational contribution or the antisymmetric rotational contribution is associated with even rotational wave numbers ($\psi_{\text{rot}}=0, 2, 4, \dots$) or odd wave numbers ($\psi_{\text{rot}}=1, 3, 5, \dots$). Dennison proved that only the symmetric rotational contribution can occupy the even levels, because this was the only combination that could explain the experimental behavior observed in the heat capacities.¹² Thus, Eq. (2) represents the even ($\psi_{\text{rot}}=0, 2, 4, \dots$) rotational energy levels associated with parahydrogen, the form prevalent at low temperatures, and Eq. (3) represents the odd ($\psi_{\text{rot}}=1, 3, 5, \dots$) rotational energy levels

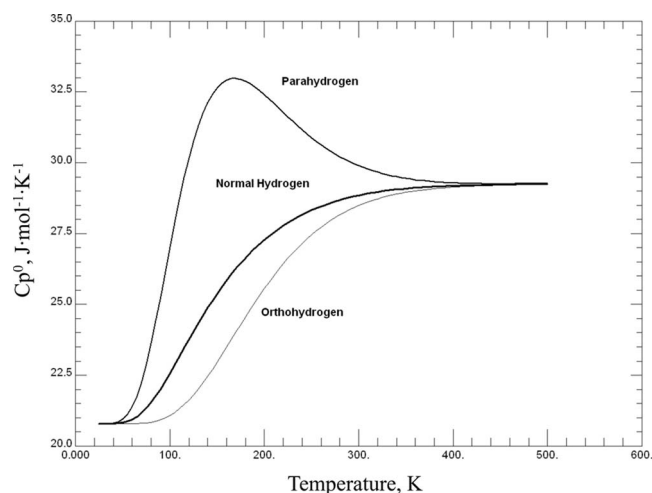


Fig. 1. Calculated ideal-gas heat capacities of parahydrogen, normal hydrogen, and orthohydrogen.

associated with orthohydrogen, the form prevalent at high temperatures.

The parahydrogen antisymmetric nuclear spin wave function has only one possible substate and is therefore called a singlet. In contrast, the higher energy symmetric nuclear spin wave function of orthohydrogen has three possible substates and is called a triplet. An equilibrium sample of hydrogen at 19 K possesses insufficient thermal energy to significantly populate higher energy states and is therefore 99.75% parahydrogen because parahydrogen has the lower energy level of the two hydrogen forms. As the temperature of an equilibrium sample is increased, more molecules populate higher energy states; for instance, at a temperature of 80 K the equilibrium concentration is approximately 50% parahydrogen and 50% orthohydrogen.¹² When an equilibrium sample approaches room temperature, enough thermal energy exists to excite all of the possible substates, giving a mixture concentration of nearly 75% orthohydrogen and 25% parahydrogen; this 3:1 distribution ratio is commonly defined as normal hydrogen. Above room temperature, each of the four possible substates will remain equally populated, maintaining the 3:1 ratio. In the absence of special catalysts or distillation techniques, orthohydrogen cannot naturally exist in a pure form.¹³

The equilibrium mixture ratio of the two forms changes

TABLE 1. Critical-point and triple-point properties for normal hydrogen and parahydrogen used in the EOS formulations of Younglove⁷

	T (K)	p (MPa)	ρ (mol dm ⁻³)
		Parahydrogen	
Critical point	32.938	1.283 77	15.556
Triple point	13.8033	0.007 042	38.215
		Normal hydrogen	
Critical point	33.19	1.315	14.94
Triple point	13.952	0.007 7	38.3

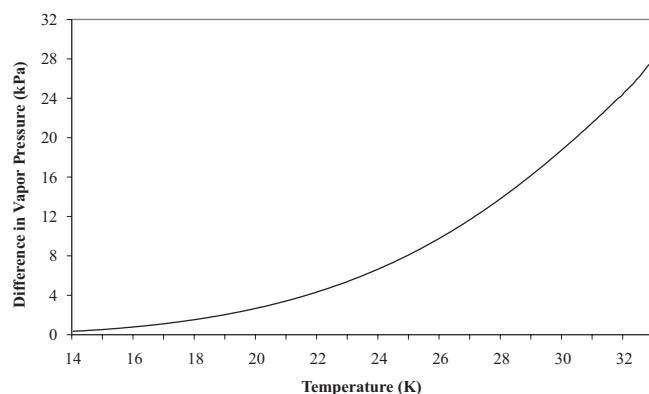


FIG. 2. Calculated vapor-pressure differences between liquid normal hydrogen and parahydrogen.

with temperature; however, it can take many days of equilibration time to achieve. Since this change generally proceeds slowly, the thermophysical properties of liquefied normal hydrogen and superheated parahydrogen can be measured. NBS Report 8812 (Ref. 14) summarizes the property differences of orthohydrogen and parahydrogen including ideal-gas values associated with caloric properties and values near and including the critical region.

The largest thermophysical property differences occur in the caloric properties for the two forms of hydrogen. Orthohydrogen and parahydrogen have considerably different rotational energies at temperatures below 250 K, with a maximum difference occurring near 145 K.¹² These differences become evident in the values of the ideal-gas heat capacities, as shown in Fig. 1. Properties such as constant-volume heat capacity, constant-pressure heat capacity, thermal conductivity, and properties derived from heat capacities such as enthalpy and entropy show significant differences between the different forms. Four sources of ideal-gas heat capacity data exist in the literature and were used in the regression of the new ideal-gas heat capacity equations to be discussed further in Secs. 4–6.^{15–18}

In addition to differences in ideal-gas properties related to heat capacity, differences in the near-critical region properties have been observed between orthohydrogen and parahydrogen.¹⁴ Since the critical region properties of pure orthohydrogen have never been measured, the previously mentioned difference is based on a sample of normal hydrogen compared to a sample of parahydrogen. The critical-point and triple-point properties used in the equations of state of Younglove⁷ for normal hydrogen and parahydrogen show this difference and are given in Table 1. These and all other temperature values reported in this work have been converted to the International Temperature Scale of 1990 (ITS-90).

Experimental vapor-pressure data for normal hydrogen and parahydrogen exhibit differences consistent with those for the critical-point and triple-point properties in Table 1. The differences between the vapor pressures of normal hydrogen and parahydrogen based on experimental vapor-pressure data are shown in Fig. 2. These near-critical prop-

TABLE 2. Values of the quantum parameter for several fluids¹⁹

Fluid	Quantum parameter Λ^*
Xenon	0.064
Krypton	0.10
Argon	0.19
Neon	0.58
Tritium	1.0–1.1
Deuterium	1.22
Hydrogen	1.73
Helium-4	2.67
Helium-3	3.08

erty differences that pertain primarily to vapor pressure and density are due to the difference in the intermolecular potential between parahydrogen and orthohydrogen.^{13,14} Because the Younglove⁷ formulations for normal hydrogen and parahydrogen use identical parameters and coefficients for the real-fluid part of the equations of state, the Younglove⁷ models do not predict different vapor pressures or densities for the different hydrogen forms excluding the critical point.

Although normal hydrogen is a 3:1 mixture of orthohydrogen and parahydrogen, nonidealities associated with the mixing of the two fluids are negligibly small. Section 6.3 lists normal hydrogen experimental data, many of which have verified concentrations. Normal hydrogen will be treated as a pure fluid for the modeling purposes of this work.

4. The Quantum Law of Corresponding States

Because of the apparent similarities in the shape of the real-fluid property surfaces for parahydrogen and normal hydrogen, one would expect the traditional molecular theory of corresponding states to yield fairly accurate transformations between the hydrogen forms. This is not the case, however, because of the quantum characteristics of hydrogen. As early as 1922, Byk and later Pitzer recognized that a primary contributor to deviations from the classical theory of corresponding states was quantum mechanical characteristics of the molecules being studied.¹⁹

As the molar mass is reduced, the deviation from classical molecular interactions increases due to the increased effect of quantum mechanics on intermolecular interactions. The classical theoretical approach to treating molecular interactions uses the Lennard-Jones 6-12 potential:

$$U = 4\epsilon \left[\left(\frac{\sigma}{r} \right)^{12} - \left(\frac{\sigma}{r} \right)^6 \right], \quad (4)$$

where r is the intermolecular distance and ϵ and σ are fluid-specific constants.¹³ The constant ϵ is the maximum well depth (J/mol) and σ is the intermolecular distance (m), where the intermolecular potential energy is zero. The first term in Eq. (4) represents the repulsion between molecules, and the second term is the attraction. In the 1940s de Boer was the first to use the interaction parameters of the Lennard-Jones

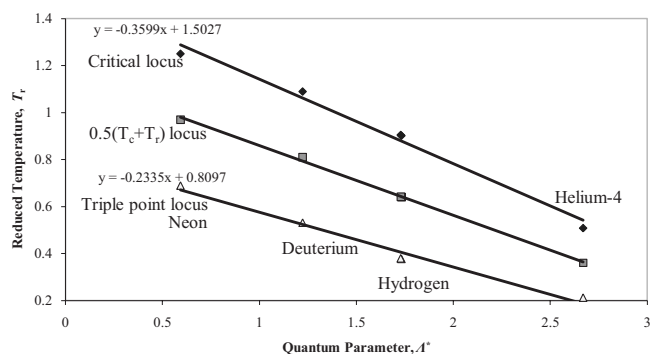


FIG. 3. Reduced temperature versus quantum parameter.

potential together with Avogadro's number, N_A , the reduced Planck constant \hbar , and the molar mass M to create a useful quantum parameter:

$$\Lambda^* = \frac{N_A 2\pi\hbar}{\sigma(M\varepsilon)^{1/2}}. \quad (5)$$

In this form the quantum parameter is analogous to a reduced de Broglie wavelength.¹⁹ The parameter was used by de Boer²⁰ to predict properties of helium-3 and later by Rogers and Brickwedde²¹ to predict properties of deuterium and tritium.

The quantum parameter gives an indication of the effect of quantum behavior on a molecular interaction. Table 2 lists the quantum parameters for several fluids.

In Table 2, there is a row labeled "Hydrogen" that is not specified as orthohydrogen or parahydrogen. Since the quantum parameter is based on the intermolecular potential, a difference in quantum parameters for orthohydrogen and parahydrogen cannot exist unless a difference in intermolecular potentials exists. Most modern statistical thermodynamics texts do not specify the difference in potential parameters between orthohydrogen and parahydrogen because the differences are small.

The differences in vapor pressures and critical-region properties established in Sec. 3 cannot be reproduced without making a distinction between the potential parameters for orthohydrogen and parahydrogen. Knaap and Beenakker²² used the differences in calculated polarizability of orthohydrogen and parahydrogen to deduce different intermolecular

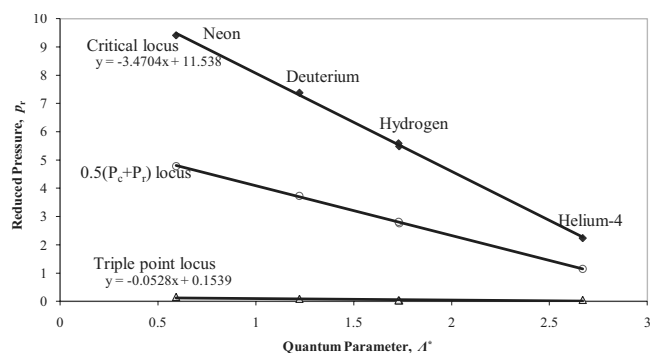


FIG. 4. Reduced pressure versus quantum parameter.

parameters applicable to data in the ground states. The difference in polarizability was based on differences in the calculated internuclear separation distance between orthohydrogen and parahydrogen in their ground rotational states. From this they found

$$\frac{\varepsilon_{\text{ortho}}}{\varepsilon_{\text{para}}} = 1.006 \quad (6)$$

and

$$\frac{\sigma_{\text{ortho}}}{\sigma_{\text{para}}} = 1.0003, \quad (7)$$

where the subscripts ortho and para denote orthohydrogen and parahydrogen, respectively. The values for normal hydrogen can be determined by linear interpolation,²³

$$\frac{\varepsilon_{\text{norm}}}{\varepsilon_{\text{para}}} = 1.0045, \quad (8)$$

$$\frac{\sigma_{\text{norm}}}{\sigma_{\text{para}}} = 1.00023. \quad (9)$$

The parameters for the Lennard-Jones potential for normal hydrogen are 36.7 J/mol for the maximum well depth ε and 2.959×10^{-10} m for the intermolecular distance σ .¹⁹ With these new parameters for the intermolecular potential, it was then possible to differentiate between properties of orthohydrogen and parahydrogen in the ground states with respect to the quantum parameter. By rewriting p , ρ , and T in terms of these constants we obtain the dimensionless quantities¹³

$$p^* = \frac{N_A \sigma^3 p}{\varepsilon}, \quad (10)$$

$$\rho^* = N_A \sigma^3 \rho, \quad (11)$$

$$T^* = \frac{RT}{\varepsilon}. \quad (12)$$

Plotting reduced thermodynamic properties versus the quantum parameter, a functional relationship between the quantum parameter and temperature, pressure, or density for light fluids can be determined. Figure 3 shows the reduced critical temperature, triple-point temperature, and the temperature of the saturated vapor halfway between the critical and triple points for the fluids neon, deuterium, normal hydrogen, parahydrogen, and helium-4. Figure 4 displays reduced pressures plotted against the quantum parameter.

Van Dael *et al.*²³ used a corresponding-states approach assuming a linear relationship between the critical temperature and quantum parameter to explain the change in critical temperatures between normal hydrogen and parahydrogen. Their equation for the reduced critical temperature of parahydrogen was

$$T_{c,\text{para}}^* = T_{c,\text{norm}}^* + (\Lambda_{\text{para}}^* - \Lambda_{\text{norm}}^*) \frac{\Delta T_c^*}{\Delta \Lambda^*}. \quad (13)$$

A similar equation using pressures or densities could also be employed. The subscripts c and t denote critical-point and triple-point properties, respectively. Figures 3 and 4 also show that the slope of a line passing through constant ratio values in between the critical and triple points can be adjusted by taking

$$\frac{\Delta T^*}{\Delta \Lambda^*} = \left(\frac{T - T_t}{T_c - T_t} \right) \left(\frac{\Delta T_c^*}{\Delta \Lambda^*} - \frac{\Delta T_t^*}{\Delta \Lambda^*} \right) + \frac{\Delta T_t^*}{\Delta \Lambda^*}, \quad (14)$$

$$\frac{\Delta p^*}{\Delta \Lambda^*} = \left(\frac{p - p_t}{p_c - p_t} \right) \left(\frac{\Delta p_c^*}{\Delta \Lambda^*} - \frac{\Delta p_t^*}{\Delta \Lambda^*} \right) + \frac{\Delta p_t^*}{\Delta \Lambda^*}, \quad (15)$$

thus enabling calculation of ground-state properties away from the critical point.

Additional properties can be found by use of combinations of reduced T , p , and ρ through dimensional analysis. For example, the reduced speed of sound can be described as²³

$$w^* = \frac{w}{\left(\frac{N_A \varepsilon}{M} \right)^{1/2}}. \quad (16)$$

If the data point includes a measured pressure and temperature, the pressure and temperature can be transformed while holding the third experimental property value (e.g., density or speed of sound) constant. The theory was tested and shown to transform data from parahydrogen to normal hydrogen within the accuracy of the existing normal hydrogen data. These comparisons are shown in Sec. 6.2.

5. Equations of State and Ancillary Equations

This section describes the functional form and procedure for the equations of state developed in this work. Sections 6.1–6.4 present comparisons of the new equations of state with the experimental data used in the fit. Only the information pertaining to the new hydrogen formulations is presented here; detailed discussions of modern thermodynamic property formulations and the methods used to develop such formulations can be found in publications such as those by Lemmon and Jacobsen⁴ and Span *et al.*⁵ The functional form of the parahydrogen, normal hydrogen, and orthohydrogen equations of state are the same, and the numerical values for the coefficients and fixed-point properties are determined through regression of primarily experimental data. Transformed data obtained with the QLCS were used in the absence of experimental data and to elucidate differing trends in the data.

The new equations of state are explicit in the Helmholtz free energy a . The Helmholtz free energy is expressed as

TABLE 3. Parameters and coefficients of the parahydrogen, normal hydrogen, and orthohydrogen ideal-gas heat capacity equations, Eq. (25)

k	Parahydrogen		Normal hydrogen		Orthohydrogen	
	u_k	v_k	u_k	v_k	u_k	v_k
1	4.302 56	499	1.616	531	2.541 51	856
2	13.028 9	826.5	-0.4117	751	-2.366 1	1444
3	-47.736 5	970.8	-0.792	1989	1.003 65	2194
4	50.001 3	1166.2	0.758	2484	1.224 47	6968
5	-18.626 1	1341.4	1.217	6859	-	-
6	0.993 973	5395	-	-	-	-
7	0.536 078	10185	-	-	-	-

$$\frac{a(T, \rho)}{RT} = \alpha(\tau, \delta), \quad (17)$$

where α is the reduced Helmholtz free energy and τ and δ are the reciprocal reduced temperature and reduced density:

$$\tau = \frac{T_c}{T}, \quad (18)$$

$$\delta = \frac{\rho}{\rho_c}. \quad (19)$$

The subscript c denotes a critical-point property. The reduced Helmholtz free energy is composed of two parts, the ideal-gas contribution α^0 and the residual contribution α^r :

$$\alpha(\tau, \delta) = \alpha^0(\tau, \delta) + \alpha^r(\tau, \delta). \quad (20)$$

The ideal contribution to the Helmholtz free energy is based on nonlinear regression of calculated ideal-gas heat capacity data from the literature. The residual contribution to the Helmholtz free energy is based on nonlinear regression of experimental thermodynamic and caloric data. Once the

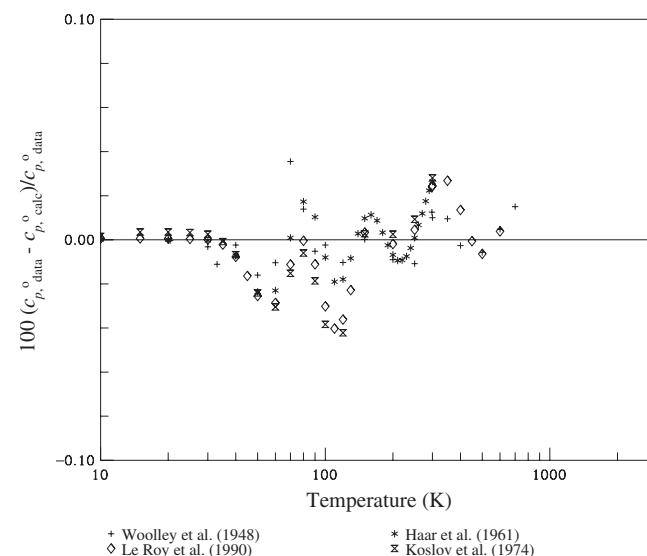


FIG. 5. Comparison of calculated ideal-gas isobaric heat capacities for parahydrogen to literature data.

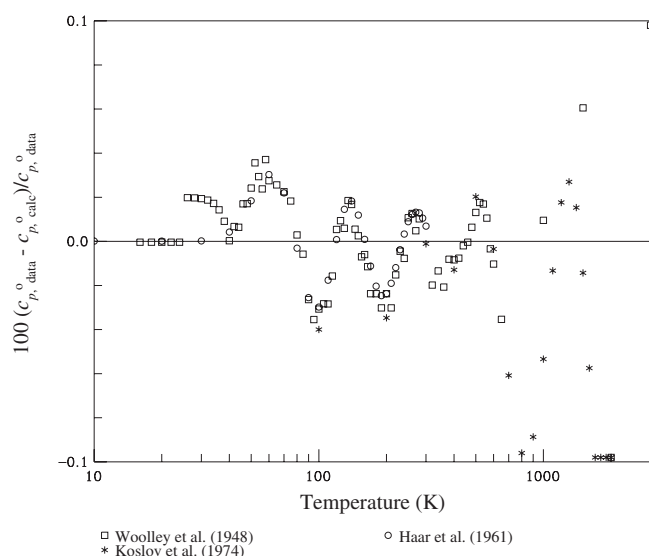


Fig. 6. Comparison of calculated ideal-gas isobaric heat capacities for normal hydrogen to literature data.

value of the reduced Helmholtz free energy is calculated, other thermodynamic properties can be calculated. Equations for calculating energies, enthalpies, entropies, heat capacities, sound speeds, etc., are given by Span *et al.*⁵ This regression process is discussed in Sec. 5.1 with the resulting coefficients and fixed-point properties discussed in Secs. 5.2–5.4.

5.1. The Regression Process

In this work, a nonlinear fitting algorithm based on the Levenberg-Marquardt method was used to optimize the ideal and residual contributions of Eq. (20).⁴ The ideal and residual contributions are composed of polynomial terms and are discussed in detail in Secs. 5.2 and 5.3, respectively. The fitting algorithm minimizes the function

$$S = \sum W_p F_p^2 + \sum W_\rho F_\rho^2 + \sum W_{c_v} F_{c_v}^2 + \dots, \quad (21)$$

where W specifies the weight assigned to a particular property and F specifies the deviation of the property from the equation being optimized and the two are summed for all of the points being fitted. A different weight W was assigned to

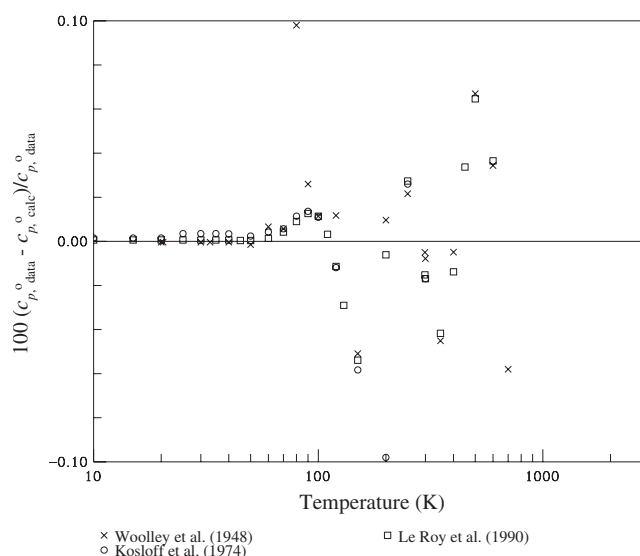


Fig. 7. Comparison of calculated ideal-gas isobaric heat capacities for orthohydrogen to literature data.

each data point used in the fitting process. Some of these deviation calculations are shown below in Eqs. (22)–(24) and similar equations are used for other properties included in the fit:

$$F_p = \frac{(p_{\text{data}} - p_{\text{calc}})}{p_{\text{data}}}, \quad (22)$$

$$F_{c_v} = \frac{(c_{v,\text{data}} - c_{v,\text{calc}})}{c_{v,\text{data}}}, \quad (23)$$

$$F_\rho = \frac{(p_{\text{data}} - p_{\text{calc}})}{\rho_{\text{data}}} \left(\frac{\partial \rho}{\partial p} \right)_T. \quad (24)$$

The quality of the resulting EOS is determined through comparison of calculated deviations of individual data points and the total deviations of specific data sets. Once the quality of the resulting EOS representation of the experimental data is assessed, new data points, numerical weights, and term combinations can be assigned to improve deficiencies. The final EOS is the result of numerous iterations of this process.

TABLE 4. Parameters and coefficients of the parahydrogen, normal hydrogen, and orthohydrogen ideal-gas Helmholtz free energy equations, Eq. (31)

k	Parahydrogen		Normal hydrogen		Orthohydrogen	
	a_k	b_k	a_k	b_k	a_k	b_k
1	-1.448 589 113 4	–	-1.457 985 647 5	–	-1.467 544 233 6	–
2	1.884 521 239	–	1.888 076 782	–	1.884 506 886 2	–
3	4.302 56	-15.149 675 147 2	1.616	-16.020 515 914 9	2.541 51	-25.767 609 873 6
4	13.028 9	-25.092 598 214 8	-0.411 7	-22.658 017 800 6	-2.366 1	-43.467 790 487 7
5	-47.736 5	-29.473 556 378 7	-0.792	-60.009 051 138 9	1.003 65	-66.044 551 475 0
6	50.001 3	-35.405 914 141 7	0.758	-74.943 430 381 7	1.224 47	-209.753 160 746 5
7	-18.626 1	-40.724 998 482	1.217	-206.939 206 516 8	–	–
8	0.993 973	-163.792 579 998 8	–	–	–	–
9	0.536 078	-309.217 317 384 2	–	–	–	–

TABLE 5. Parameters and coefficients of the new parahydrogen, normal hydrogen, and orthohydrogen equations of state

<i>i</i>	Parahydrogen				Normal hydrogen				Orthohydrogen			
	N_i	t_i	d_i	p_i	N_i	t_i	d_i	p_i	N_i	t_i	d_i	p_i
1	-7.333 75	0.6855	1	0	-6.936 43	0.6844	1	0	-6.831 48	0.7333	1	0
2	0.01	1	4	0	0.01	1	4	0	0.01	1	4	0
3	2.603 75	1	1	0	2.110 1	0.989	1	0	2.115 05	1.1372	1	0
4	4.662 79	0.489	1	0	4.520 59	0.489	1	0	4.383 53	0.5136	1	0
5	0.682 390	0.774	2	0	0.732 564	0.803	2	0	0.211 292	0.5638	2	0
6	-1.470 78	1.133	2	0	-1.340 86	1.1444	2	0	-1.009 39	1.6248	2	0
7	0.135 801	1.386	3	0	0.130 985	1.409	3	0	0.142 086	1.829	3	0
8	-1.053 27	1.619	1	1	-0.777 414	1.754	1	1	-0.876 96	2.404	1	1
9	0.328 239	1.162	3	1	0.351 944	1.311	3	1	0.804 927	2.105	3	1
10	-0.057 783 3	3.96	2	-	-0.021 171 6	4.187	2	-	-0.710 775	4.1	2	-
11	0.044 974 3	5.276	1	-	0.022 631 2	5.646	1	-	0.063 968 8	7.658	1	-
12	0.070 346 4	0.99	3	-	0.032 187	0.791	3	-	0.071 085 8	1.259	3	-
13	-0.040 176 6	6.791	1	-	-0.023 175 2	7.249	1	-	-0.087 654	7.589	1	-
14	0.119 510	3.19	1	-	0.055 734 6	2.986	1	-	0.647 088	3.946	1	-

5.2. Ideal-Gas Contributions to the Reduced Helmholtz Free Energy

The ideal-gas heat capacity equation is expressed as

$$\frac{c_p^0}{R} = 2.5 + \sum_{k=1}^N u_k \left(\frac{v_k}{T} \right)^2 \frac{\exp(v_k/T)}{[\exp(v_k/T) - 1]^2}, \quad (25)$$

where the parameters and coefficients of the equation are given in Table 3. The parameters and coefficients were regressed to the most accurate predictions available of the ideal-gas isobaric heat capacity.¹⁵⁻¹⁸ The percentage deviations between the calculated values from Eq. (25) and the literature values are shown in Fig. 5 for parahydrogen, Fig. 6 for normal hydrogen, and Fig. 7 for orthohydrogen. The correlations are valid from nearly 0 to 1000 K and the estimated uncertainty of the formulations is less than 0.04% for parahydrogen, less than 0.1% for normal hydrogen, and less than 0.1% for orthohydrogen.

The ideal-gas Helmholtz free energy is

$$a^0 = h^0 - RT - Ts^0, \quad (26)$$

where the ideal-gas enthalpy is

$$h^0 = h_0^0 + \int_{T_0}^T c_p^0 dT, \quad (27)$$

and the ideal-gas entropy is

$$s^0 = s_0^0 + \int_{T_0}^T \frac{c_p^0}{T} dT - R \ln \left(\frac{\rho T}{\rho_0 T_0} \right). \quad (28)$$

Combining Eqs. (26)–(28) gives

$$a^0 = h_0^0 + \int_{T_0}^T c_p^0 dT - RT - T \left[s_0^0 + \int_{T_0}^T \frac{c_p^0}{T} dT - R \ln \left(\frac{\rho T}{\rho_0 T_0} \right) \right], \quad (29)$$

and in reduced form

TABLE 6. Parameters of the Gaussian terms in the new parahydrogen, normal hydrogen, and orthohydrogen equations of state

<i>i</i>	φ_i	β_i	γ_i	D_i
Parahydrogen				
10	-1.7437	-0.194	0.8048	1.5487
11	-0.5516	-0.2019	1.5248	0.1785
12	-0.0634	-0.0301	0.6648	1.28
13	-2.1341	-0.2383	0.6832	0.6319
14	-1.777	-0.3253	1.493	1.7104
Normal hydrogen				
10	-1.685	-0.171	0.7164	1.506
11	-0.489	-0.2245	1.3444	0.156
12	-0.103	-0.1304	1.4517	1.736
13	-2.506	-0.2785	0.7204	0.67
14	-1.607	-0.3967	1.5445	1.662
Orthohydrogen				
10	-1.169	-0.4555	1.5444	0.6366
11	-0.894	-0.4046	0.6627	0.3876
12	-0.04	-0.0869	0.763	0.9437
13	-2.072	-0.4415	0.6587	0.3976
14	-1.306	-0.5743	1.4327	0.9626

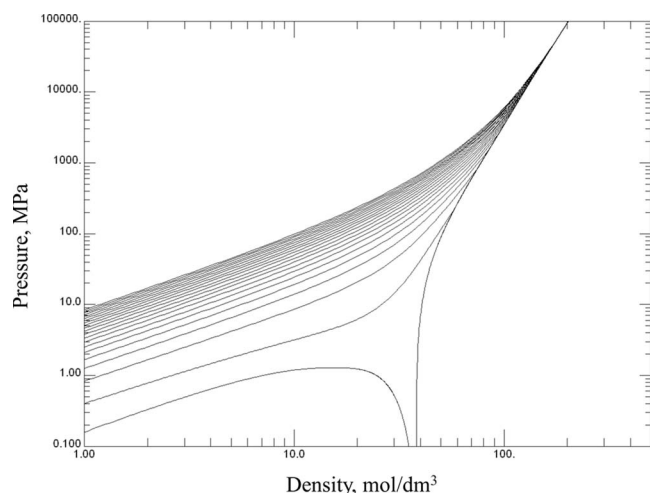


FIG. 8. Predicted pressures versus densities at extreme conditions for the new parahydrogen EOS.

$$\alpha^0 = \frac{h_0^0 \tau}{RT_c} - \frac{s_0^0}{R} - 1 + \ln \frac{\delta \tau_0}{\delta_0 \tau} - \frac{\tau}{R} \int_{\tau_0}^{\tau} \frac{c_p^0}{\tau^2} d\tau + \frac{1}{R} \int_{\tau_0}^{\tau} \frac{c_p^0}{\tau} d\tau, \quad (30)$$

where $\delta_0 = \rho_0 / \rho_c$ and $\tau_0 = T_c / T_0$. A computationally convenient parametrized form of Eq. (30) is

$$\alpha^0 = \ln \delta + 1.5 \ln \tau + a_1 + a_2 \tau + \sum_{k=3}^N a_k \ln[1 - \exp(b_k \tau)]. \quad (31)$$

The subscript k is the index of each term in the ideal-gas heat capacity equation. The ideal-gas heat capacity coefficients a_k and b_k used in the new formulations for parahydrogen, normal hydrogen, and orthohydrogen are listed in Table 4.

5.3. Residual Contribution to the Reduced Helmholtz Free Energy

The residual contribution to the reduced Helmholtz free energy is

$$\begin{aligned} \alpha^r(\tau, \delta) = & \sum_{i=1}^l N_i \delta^{d_i} \tau^{t_i} + \sum_{i=l+1}^m N_i \delta^{d_i} \tau^{t_i} \exp(-\delta^{p_i}) \\ & + \sum_{i=m+1}^n N_i \delta^{d_i} \tau^{t_i} \exp[\varphi_i(\delta - D_i)^2 + \beta_i(\tau - \gamma_i)^2]. \end{aligned} \quad (32)$$

For the new equations of state, the first summation is a simple polynomial comprising seven terms, with exponents d_i and t_i on the reduced density and temperature, respectively. The second summation contains an exponential density component to aid in liquid and critical-region property calculations and consists of two terms. The third summation contains five modified Gaussian bell-shaped terms. The purpose of the Gaussian bell-shaped terms is to improve modeling of the critical region. The critical region is the most

TABLE 7. Critical- and triple-point properties used by the new parahydrogen, normal hydrogen, and orthohydrogen equations of state (this work)

	Temperature (K)	Pressure (MPa)	Density (mol dm ⁻³)
Parahydrogen			
Critical point	32.938	1.285 8	15.538
Triple point	13.8033	0.007 041	38.185
Normal hydrogen			
Critical point	33.145	1.296 4	15.508
Triple point	13.957	0.007 36	38.2
Orthohydrogen			
Critical point	33.22	1.310 65	15.445
Triple point	14.008	0.007 461	38.2

difficult to measure experimentally and is the most difficult to model.

Although the values of N_i , d_i , t_i , p_i , φ_i , β_i , γ_i , and D_i are somewhat arbitrary, bounds on some of their values were set to obtain physically correct equation behavior. The values of d_i , p_i , t_i , γ_i , and D_i are positive and those of d_i and p_i are integers. The values of φ_i and β_i are negative. For these equations of state $l=7$, $m=9$, and $n=14$.

The simple polynomial terms for the new parahydrogen, normal hydrogen, and orthohydrogen equations of state are given in Table 5. The modified Gaussian terms for each fluid are given in Table 6.

To correctly extrapolate the isothermal behavior at high densities for the new parahydrogen EOS, the term with $t=1$ and $d=4$ with a positive coefficient was chosen for the polynomial term with the highest d value. This term is dominant at high densities. The use of the $t=1$ term eliminates the temperature dependence at extreme conditions. If a value less than 1 was used, the isotherms would become parallel, and a value greater than 1 would cause the isotherms to cross. The analytical details of this approach are given elsewhere.⁴ Figure 8 shows the isothermal behavior of the new parahydrogen EOS at extreme temperatures, pressures, and densities.

To test the thermodynamic consistency of the final functional form of the equation of state, plots of certain characteristic properties were created. The curvatures of the Boyle curve, ideal curve, Joule-Thomson inversion curve, and Joule inversion curve must be monotonic. The new parahydrogen, normal hydrogen, and orthohydrogen equations of state have monotonic characteristic curves of forms similar to those described by Lemmon and Jacobsen.⁴

The parahydrogen EOS was regressed first because the available parahydrogen experimental data, discussed in detail in Sec. 6.1, were the most consistent, the most complete near the critical region, and the most verified orthohydrogen-parahydrogen concentration. To create the new normal hydrogen EOS, the QLCS was applied to the primary parahydrogen experimental data below 60 K as well as to certain predictions of the parahydrogen EOS, which will be discussed in Secs. 6.2 and 6.3. With the QLCS predictions and

TABLE 8. Parameters and coefficients of the parahydrogen, normal hydrogen, and orthohydrogen vapor pressure ancillary equations, Eq. (33)

<i>i</i>	Parahydrogen		Normal hydrogen		Orthohydrogen	
	N_i	k_i	N_i	k_i	N_i	k_i
1	-4.877 67	1	-4.897 89	1	-4.886 84	1
2	1.033 59	1.5	0.988 558	1.5	1.053 10	1.5
3	0.826 68	2.65	0.349 689	2	0.856 947	2.7
4	-0.129 412	7.4	0.499 356	2.85	-0.185 355	6.2

the available normal hydrogen experimental data, the new normal hydrogen EOS was created. Then the new orthohydrogen EOS was regressed from transformed parahydrogen data by regressing the new normal hydrogen EOS to pure orthohydrogen data predicted using the QLCS.

5.4. Fixed-Point Properties

It is possible to use nonlinear regression techniques to determine the critical-point properties based on other critical-region data as part of the optimization process. As a result,

the calculated critical point for the EOS may not exactly match a particular selected experimental critical point of the actual fluid; however, the final value will generally lie within the uncertainties of published experimental values. There are some instances where the predicted critical state may be considered more accurate than measured values, but no generalization of this behavior has been made.

The critical properties from the Younglove⁷ equations of state were used as initial starting points in the nonlinear regression and are shown in Table 1. Since the critical-point values were treated as adjustable parameters with this fitting technique, the critical-point values determined by the regression for the new formulations changed slightly from those of the Younglove⁷ models. The current EOS was published by Younglove⁷ in 1985, before the new ITS-90 temperature scale was adopted. On the ITS-90 scale, the triple point of parahydrogen is a fixed point, and the new parahydrogen EOS is consistent with this point. The critical and triple-point values used in this work are given in Table 7.

The critical density is difficult to reproduce experimentally because of the small change in slope of the critical isotherm very near the critical pressure. The critical densities of nor-

TABLE 9. Parahydrogen experimental data sets and AAD from the new and Younglove⁷ equations of state

Reference	Rank	Total points	T (K)	p (MPa)	AAD from new EOS	AAD from Younglove ⁷
p - ρ - T						
Goodwin <i>et al.</i> (1963) ⁴¹	1	1234	15–100	1.5–35.5	0.18	0.36
Goodwin <i>et al.</i> (1961) ⁴²	2	17	17.0–33.0	sat	0.41	0.88
Hoge and Lassiter (1951) ⁴⁹	2	46	32.9–33.3	1.3–1.4	3.16	4.41
Roder <i>et al.</i> (1963) ⁷³	1	46	33.0–40.0	1.3–2.8	1.28	2.33
Isochoric heat capacity						
Younglove and Diller (1962) ⁹⁴	1	162	19.9–90.4	1.1–63.26	0.62	1.24
Isobaric heat capacity						
Medvedev <i>et al.</i> (1971) ⁶⁴	2	319	20.9–50.3	0.2–3.04	4.87	4.56
Saturation heat capacity						
Brouwer <i>et al.</i> (1970) ³⁴	2	12	24.5–30.0	sat	1.04	0.73
Smith <i>et al.</i> (1954) ⁷⁹	2	8	18.3–31.5	sat	1.85	1.04
Johnston <i>et al.</i> (1950) ⁵³	1	16	12.7–19.0	sat	0.97	2.45
Younglove and Diller (1962) ⁹⁵	1	32	14.8–31.5	sat	1.07	2.73
Vapor pressure						
Barber and Horsford (1963) ²⁸	2	10	13.8–20.3	sat	0.14	0.20
Hoge and Arnold (1951) ⁴⁸	2	45	15.8–32.9	sat	0.12	0.16
Keesom <i>et al.</i> (1931) ⁵⁶	2	31	17.2–20.5	sat	1.05	1.17
Kemp and Kemp (1979) ⁶	1	3	13.8–20.3	sat	0.34	0.40
van Itterbeek <i>et al.</i> (1964) ⁸⁶	2	42	20.6–32.3	sat	1.95	2.22
Weber <i>et al.</i> (1962) ⁸⁹	1	32	20.3–32.7	sat	0.05	0.32
Speed of sound						
Younglove (1965) ⁹³	1	251	14.5–100.0	sat–32.0	0.32	1.58
van Dael <i>et al.</i> (1965) ²³	1	23	20.3–32.0	sat	0.63	4.25
van Itterbeek <i>et al.</i> (1961) ⁸⁴	1	48	14.1–20.4	sat	0.43	2.88
van Itterbeek <i>et al.</i> (1963) ⁸³	1	116	15.1–20.5	sat–23.5	0.66	1.52
Second virial coefficient						
Goodwin <i>et al.</i> (1964) ⁴⁰	1	58	15.0–423.2	–	1.16	0.78
Third virial coefficient						
Goodwin <i>et al.</i> (1964) ⁴⁰	1	52	20.0–423.2	–	0.26	0.29

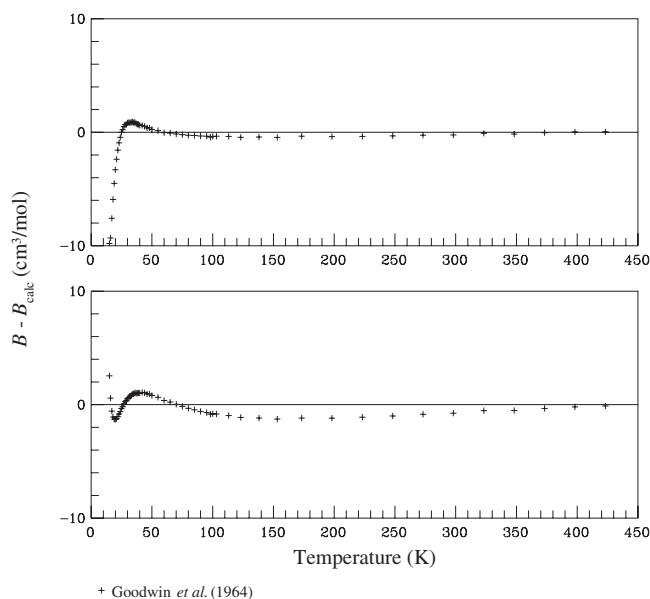


FIG. 9. Comparison of calculated second virial coefficients plotted versus temperature for the new parahydrogen EOS (top) and the parahydrogen EOS of Younglove (bottom) to experimental data.

mal hydrogen and orthohydrogen have never been measured, and the value for normal hydrogen was based on an approximation from available saturation data.^{1,7,13,15,24} To increase the accuracy of the critical density for parahydrogen, the rectilinear diameter method was used as an estimate in addition to the experimental data. To improve the accuracy of the normal hydrogen surface of state near the critical point, the QLCS was used to predict normal hydrogen values by transforming parahydrogen experimental data near the critical point to the normal hydrogen surface.

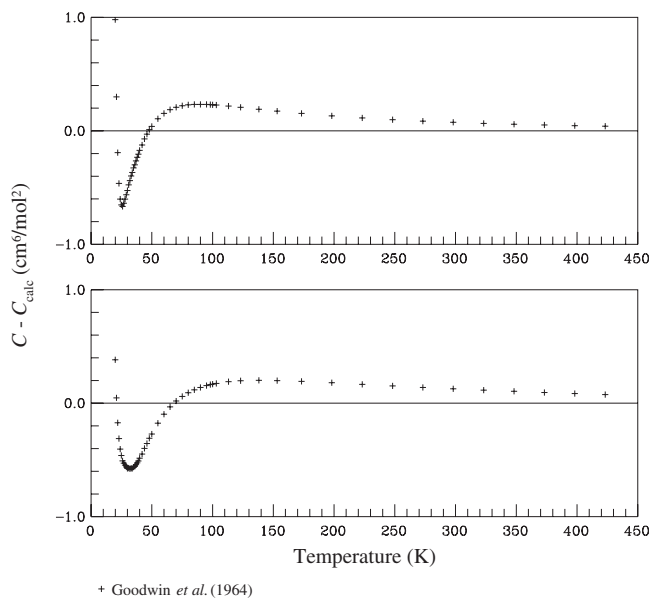


FIG. 10. Comparison of calculated third virial coefficients plotted versus temperature for the new parahydrogen EOS (top) and the parahydrogen EOS of Younglove (bottom) to experimental data.

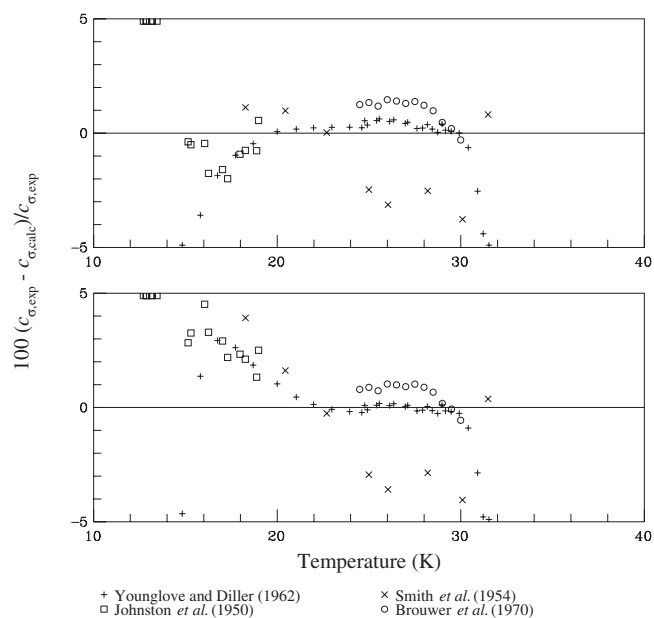


FIG. 11. Comparison of calculated saturation heat capacities for the new parahydrogen EOS (top) and the parahydrogen EOS of Younglove (bottom) to experimental data.

5.5. Vapor Pressures

It is convenient to use an ancillary equation to approximate the saturation line predicted by the Maxwell criterion with Eq. (32).⁴ The vapor pressure at saturation can be represented with the ancillary equation

$$\ln\left(\frac{p_\sigma}{p_c}\right) = \frac{T_c}{T} \sum_{i=1}^4 N_i \theta^{k_i}, \quad (33)$$

where $\theta = (1 - T/T_c)$, p_σ is the saturated vapor pressure, and the values of the coefficients N_i and the exponents k_i are given in Table 8.

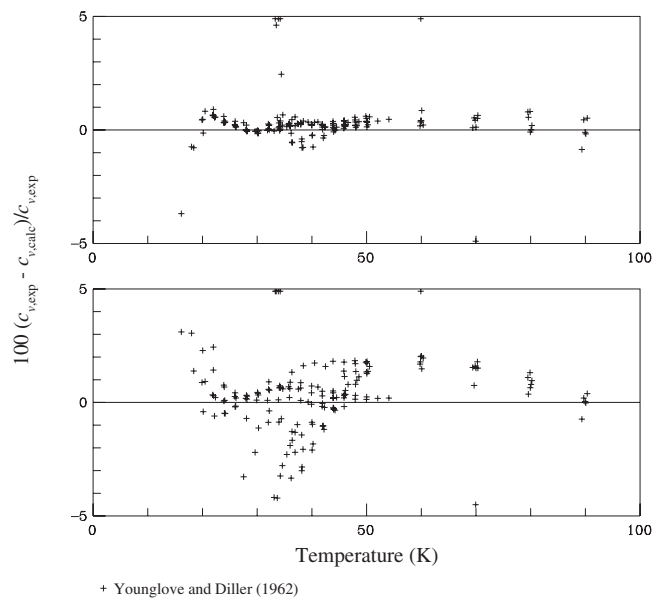


FIG. 12. Comparison of calculated isochoric heat capacities for the new parahydrogen EOS (top) and the parahydrogen EOS of Younglove (bottom) to experimental data.

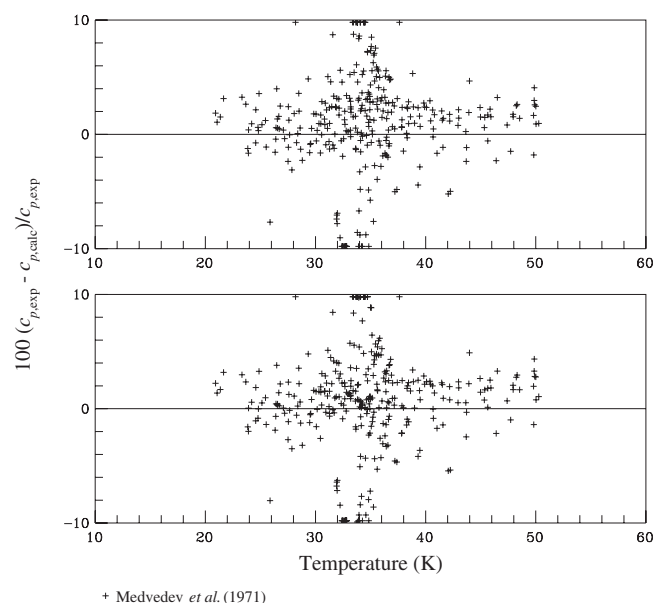


FIG. 13. Comparison of calculated isobaric heat capacities for the new parahydrogen EOS (top) and the parahydrogen EOS of Younglove (bottom) to experimental data.

6. Comparison of Calculated Data to Experimental Data

To illustrate the accuracy of an EOS, plots are created to compare property values calculated from the EOS and experimental values. In this section, comparisons are shown for calculations with the Younglove⁷ EOS in the bottom or right of each figure and the new EOS in the top or left of each figure. Some normal hydrogen density data were included in

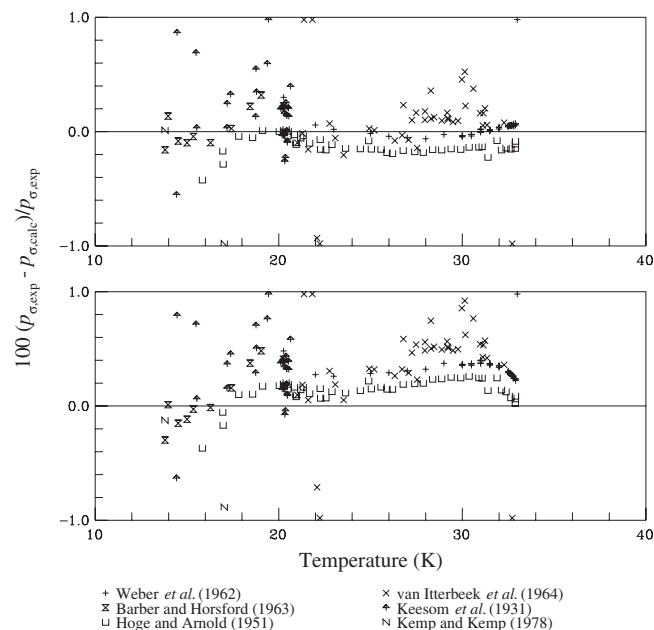


FIG. 14. Comparison of calculated vapor pressures for the new parahydrogen EOS (top) and the parahydrogen EOS of Younglove (bottom) to experimental data.

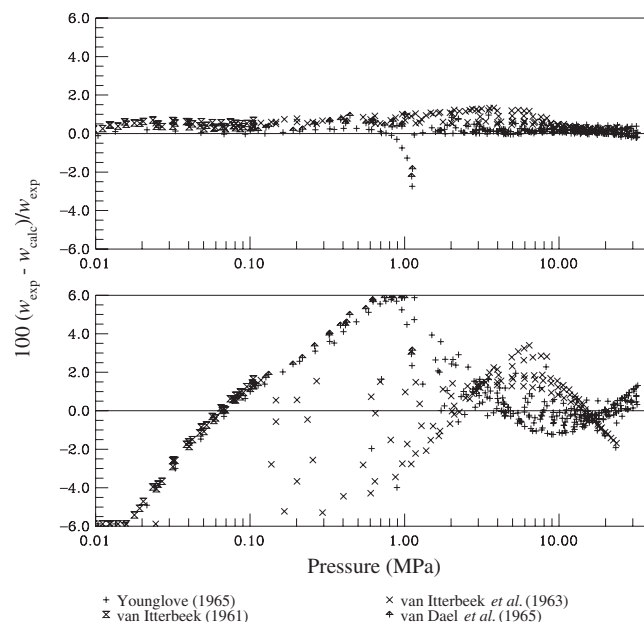


FIG. 15. Comparison of calculated sound speeds for the new parahydrogen EOS (top) and the parahydrogen EOS of Younglove (bottom) to experimental data.

the plots of parahydrogen density and pressure deviations to illustrate the differences between the densities of parahydrogen and normal hydrogen.

The absolute average deviation (AAD) for each data set is calculated by

$$\text{AAD} = \frac{1}{n} \sum_{i=1}^n |\% \Delta X_i|, \quad (34)$$

$$\% \Delta X = 100 \left(\frac{X_{\text{data}} - X_{\text{calc}}}{X_{\text{data}}} \right). \quad (35)$$

The second and third virial coefficients are compared with absolute average differences. Tables are included in each subsection listing the experimental data used in the regression in addition to the AAD for the new and Younglove⁷ equations of state. In the tables and figures in this section, the experimental data used in this work²⁵⁻⁹⁵ are referred to by the author(s) and year of publication.

6.1. Comparison of Calculated Parahydrogen Data to Experimental Data

Table 9 lists the experimental data sets available for parahydrogen. The names of the experimentalists are given in the “Reference” column; the ranks or priorities of the data sets are given in the second column; the number of data points and temperature and pressure ranges of the sets are given in columns 3–5; the AAD from the new and old equations of state are given in the last two columns. The rank (1 is primary, 2 is secondary) of the data set is determined based on the reputation of the laboratory, agreement with other data sets, apparatus used for the measurements, and the year the data were taken.

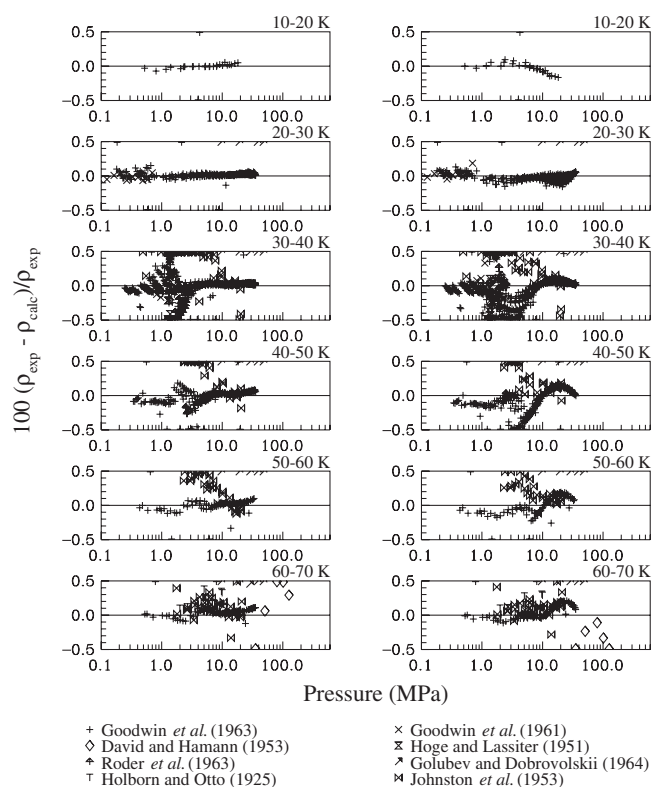


Fig. 16. Comparison of calculated densities for the new parahydrogen EOS (left) and the parahydrogen EOS of Younglove (right) to experimental data (data displayed in 10 K increments from 10 to 70 K).

Figure 9 shows the differences in second virial coefficients, and Fig. 10 shows the differences in third virial coefficients. No attempt to regress the equations of state to experimental virial-coefficient data was made, meaning that the new parahydrogen EOS representation of the virial-coefficient data is based only on representation of the p - ρ - T data.

Figures 11–13 show deviations in saturation heat capacity, isochoric heat capacity, and isobaric heat capacity. The saturation heat capacity data sets display differing trends below 20 K. Because of this difference, none of the experimental saturation heat capacity data below 20 K were used in the regression in order to allow other properties such as speed of sound to determine the curvature of the surface of state in this region. There is only one set of isochoric heat capacity data for parahydrogen available in the literature,⁹⁵ and the data were taken on the same apparatus as the saturation heat capacity data of the same group. One set of isobaric parahydrogen heat capacity data exists in the literature;⁶⁴ the precision of the data is quite low, however, and despite efforts, no discernible trend could be observed in the data.

Figure 14 compares the calculated parahydrogen vapor pressures to experimental data. In the 21–32.8 K range, the Weber *et al.*⁸⁹ data set was chosen as primary. In the 13.8–21 K range, two of the three data points of Kemp and Kemp⁶ were chosen as primary. The data set of Kemp and Kemp⁶ was used to define fixed points on the ITS-90 temperature scale, and the normal boiling point for the fit was

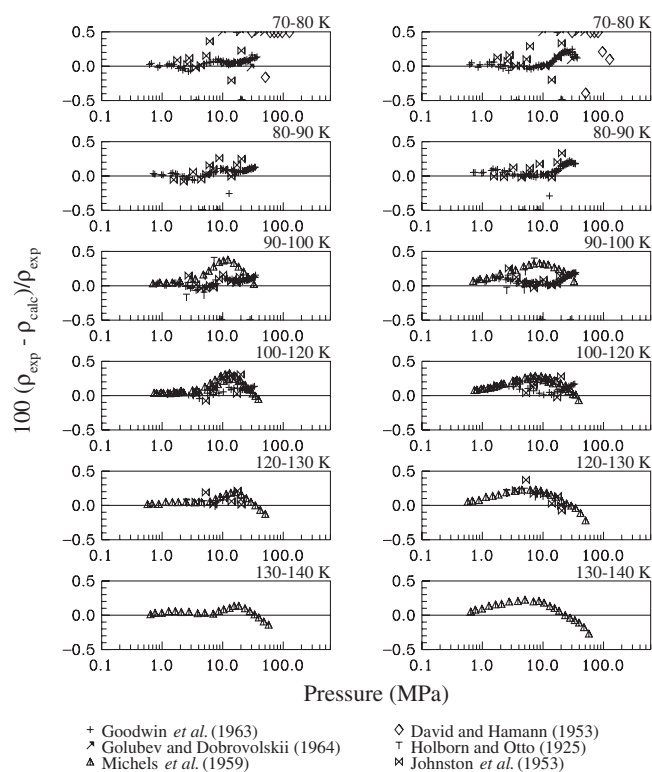


Fig. 17. Comparison of calculated densities for the new parahydrogen EOS (left) and the parahydrogen EOS of Younglove (right) to experimental data (data displayed in 10 K increments from 70 to 140 K).

selected from this set. Comparisons to the deviations of the Younglove⁷ parahydrogen EOS indicate a significant improvement in the representation with the new EOS developed in this work.

Speed-of-sound deviations for the new and Younglove⁷ parahydrogen equations of state are shown in Fig. 15. The Younglove⁹³ data were chosen as primary along the saturated liquid line and at temperatures higher than the critical temperature. The change in the deviation plot for the Younglove⁷ (bottom) and the new EOS (top) suggests a significant improvement in the representation of the data with the new parahydrogen EOS. Values of the speed of sound near the critical pressure exhibit significant deviations, possibly because of the lack of critical enhancement terms in the equations of state that could aid the speed of sound to approach zero at the critical point.

Figures 16–21 display density deviations plotted versus pressure and are separated into increments of temperature, as noted in the upper right corner of each graph. In most of the plots, the new EOS displays significant improvement over the Younglove⁷ parahydrogen EOS. In the 60–70 K plot of Fig. 16, the differences between the parahydrogen and normal hydrogen experimental density data become undetectable among available data sets. Above 70 K, normal hydrogen density data were assumed to be valid for use as parahydrogen data for the purposes of regression. In the 90–100 K plot of Fig. 17, the data of Michels *et al.*,⁶⁵ which were taken as primary at higher temperatures, deviate systematically from the data of Goodwin *et al.*,⁴¹ which were

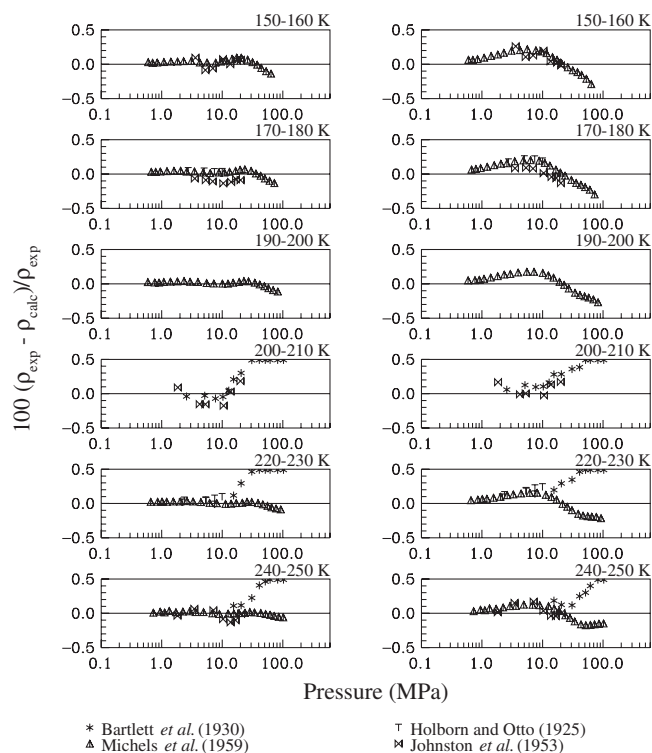


Fig. 18. Comparison of calculated densities for the new parahydrogen EOS (left) and the parahydrogen EOS of Younglove (right) to experimental data (data displayed in 10 K increments from 150 to 250 K).

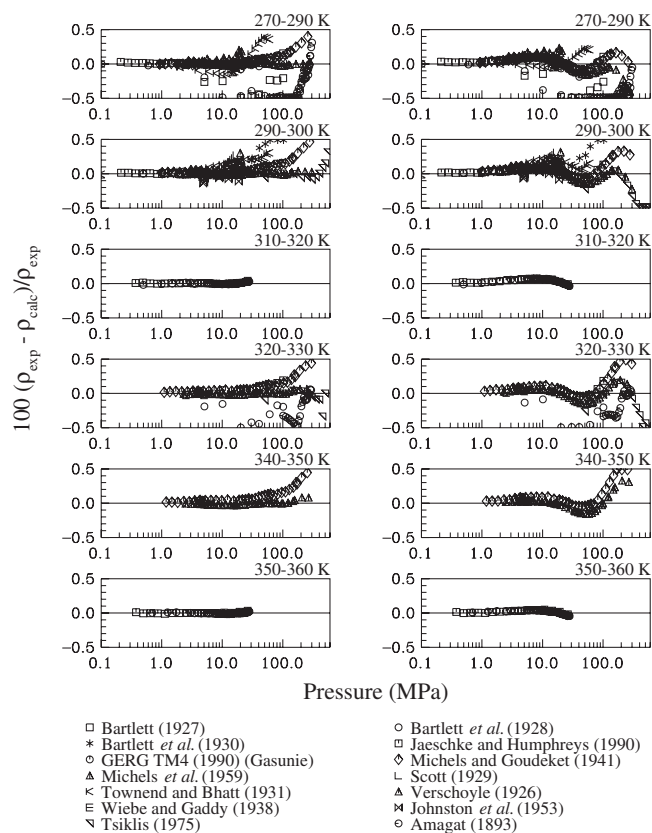


Fig. 19. Comparison of calculated densities for the new parahydrogen EOS (left) and the parahydrogen EOS of Younglove (right) to experimental data (data displayed in 10 K increments from 270 to 360 K).

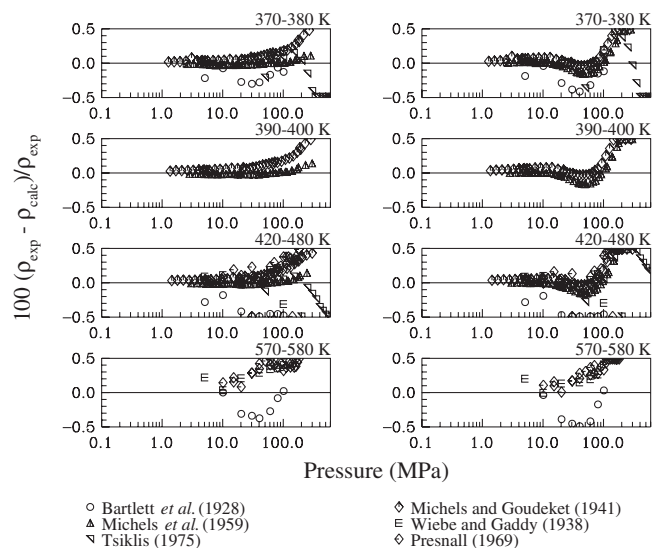


Fig. 20. Comparison of calculated densities for the new parahydrogen EOS (left) and the parahydrogen EOS of Younglove (right) to experimental data (data displayed in listed increments from 370 to 580 K).

considered primary at lower temperatures. The normal hydrogen data of Johnston *et al.*⁵⁵ trend with the Goodwin *et al.*⁴¹ data. All three apparatus used were similar in construction, so the cause of the deviation cannot be explained through differences in the experiments. Figures 22 and 23 display all of the density data on a single plot to show that the new parahydrogen EOS more accurately reproduces the high-pressure data of Liebenberg *et al.*^{59,60} The representation of the high-temperature data of Presnall⁷² could not be improved because all attempts to do so created discrepancies with the primary data of Michels *et al.*⁶⁵ Figures 22 and 23 indicate significant deviations in the current Younglove⁷ EOS from these data sets and illustrate the lack of agreement among the data at these high pressures. The cause of these errors is likely due to the incorrect behavior of the isotherms of the Younglove⁷ EOS, including some instances where the isotherms cross each other at high temperatures.

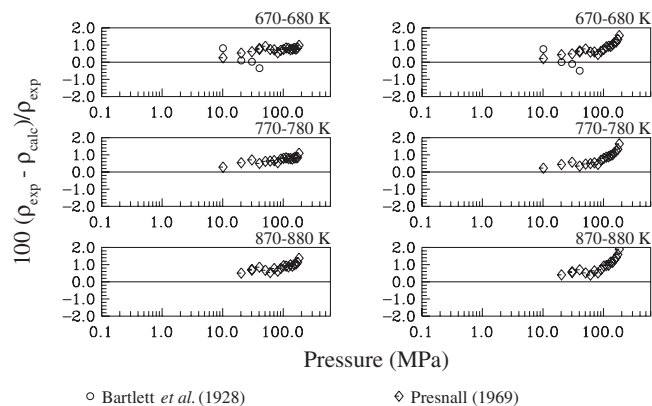


Fig. 21. Comparison of calculated densities for the new parahydrogen EOS (left) and the parahydrogen EOS of Younglove (right) to experimental data (data displayed in 10 K increments from 670 to 880 K).

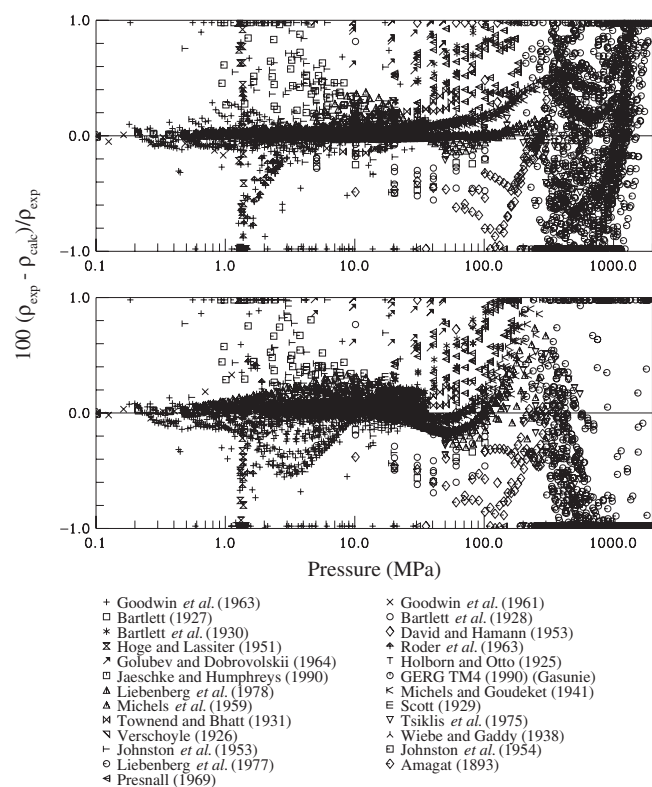


FIG. 22. Comparison of calculated densities for the new parahydrogen EOS (top) and the parahydrogen EOS of Younglove (bottom) to experimental data (data plotted against pressure).

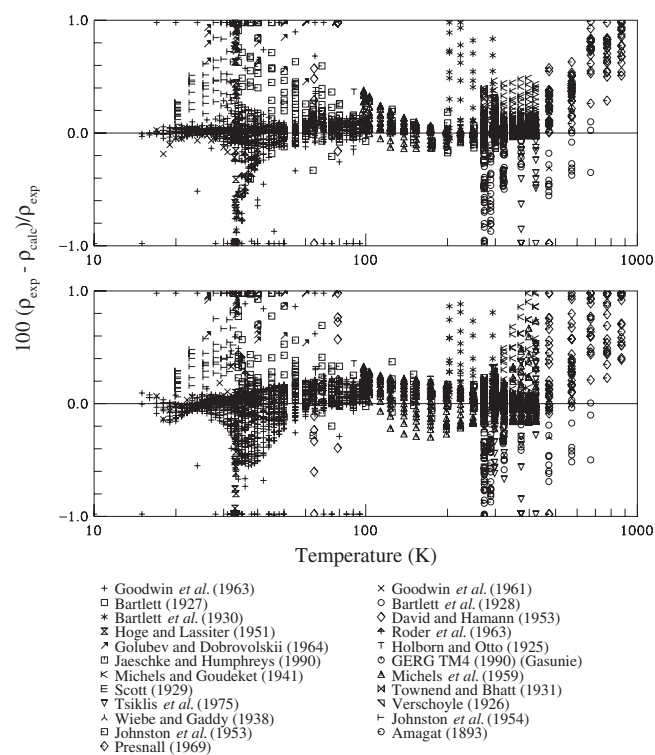


FIG. 23. Comparison of calculated densities for the new parahydrogen EOS (top) and the parahydrogen EOS of Younglove (bottom) to experimental data (data plotted against temperature).

TABLE 10. Calculated parahydrogen vapor-pressure data (this work) and the data transformed to the normal hydrogen and orthohydrogen surfaces of state

Parahydrogen (original)		Normal hydrogen		Orthohydrogen	
Temp. (K)	Pressure (MPa)	Temp. (K)	Pressure (MPa)	Temp. (K)	Pressure (MPa)
15	0.013 452	15.0989	0.013 582	15.1079	0.013 583
15.5	0.017 154	15.6016	0.017 311	15.6108	0.017 311
16	0.021 578	16.1044	0.021 768	16.1137	0.021 765
16.5	0.026 809	16.6071	0.027 039	16.6166	0.027 032
17	0.032 932	17.1099	0.033 207	17.1195	0.033 198
17.5	0.040 038	17.6126	0.040 366	17.6224	0.040 352
18	0.048 216	18.1154	0.048 606	18.1253	0.048 587
18.5	0.057 559	18.6181	0.058 019	18.6282	0.057 997
19	0.068 162	19.1209	0.068 701	19.1311	0.068 676
19.5	0.080 119	19.6237	0.080 747	19.6340	0.080 722
20	0.093 526	20.1264	0.094 255	20.1369	0.094 23
20.5	0.108 48	20.6292	0.109 32	20.6397	0.109 30
21	0.125 08	21.1319	0.126 05	21.1426	0.126 04
21.5	0.143 43	21.6347	0.144 53	21.6455	0.144 53
22	0.163 61	22.1374	0.164 86	22.1484	0.164 90
22.5	0.185 75	22.6402	0.187 17	22.6513	0.187 23
23	0.209 92	23.1429	0.211 52	23.1542	0.211 62
23.5	0.236 25	23.6457	0.238 05	23.6571	0.238 19
24	0.264 82	24.1484	0.266 83	24.1600	0.267 03
24.5	0.295 75	24.6512	0.297 99	24.6629	0.298 24
25	0.329 13	25.1539	0.331 62	25.1658	0.331 95
25.5	0.365 08	25.6567	0.367 84	25.6687	0.368 25
26	0.403 71	26.1594	0.406 76	26.1716	0.407 25
26.5	0.445 11	26.6622	0.448 47	26.6745	0.449 05
27	0.489 41	27.1649	0.493 10	27.1774	0.493 77
27.5	0.536 72	27.6677	0.540 76	27.6803	0.541 53
28	0.587 16	28.1704	0.591 58	28.1832	0.592 44
28.5	0.640 85	28.6732	0.645 67	28.6861	0.646 62
29	0.697 93	29.1760	0.703 18	29.1890	0.704 19
29.5	0.758 54	29.6787	0.764 24	29.6919	0.765 30
30	0.822 83	30.1815	0.829 01	30.1948	0.830 09
30.5	0.890 97	30.6842	0.897 66	30.6977	0.898 71
31	0.963 16	31.1870	0.970 39	31.2006	0.971 36
31.5	1.039 6	31.6897	1.047 4	31.7035	1.048 2
32	1.120 6	32.1925	1.129 0	32.2064	1.129 7
32.5	1.206 6	32.6952	1.215 7	32.7093	1.216 0

6.2. Comparison of Data Predicted Using the Quantum Law of Corresponding States

To test the QLCS, calculated vapor pressures from the new parahydrogen EOS were transformed to the normal hydrogen surface of state for comparison to existing normal hydrogen vapor-pressure data. The new parahydrogen EOS uses vapor pressure, speed-of-sound data along the saturation line, saturated heat capacity, and saturated liquid density data simultaneously to locate the saturation boundary; because of this, values calculated from the new parahydrogen EOS were chosen for transformation over experimental parahydrogen vapor-pressure data. The comparisons between the new parahydrogen EOS and experimental data are shown in Fig.

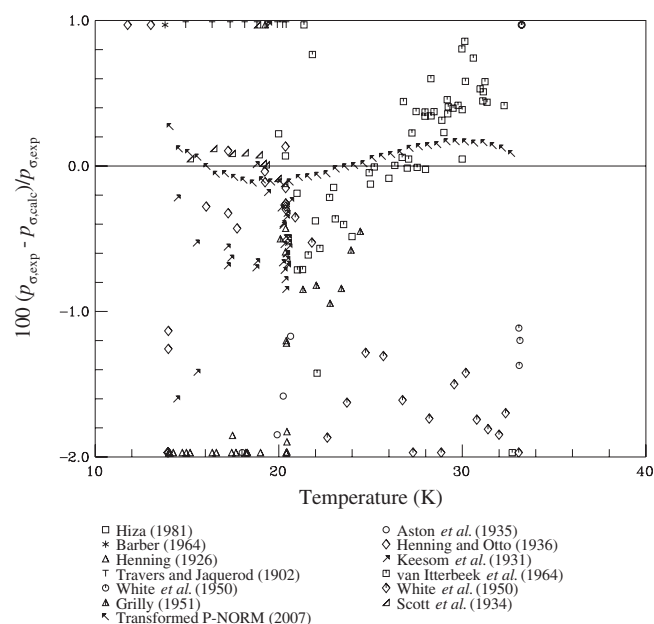


FIG. 24. Comparison of calculated vapor pressures for the new normal hydrogen EOS to experimental and predicted data.

14. Selected calculated saturated vapor-pressure data and the values transformed to the normal hydrogen and orthohydrogen surfaces of state are given in Table 10.

To test the accuracy of the transformation, the predicted vapor pressures for normal hydrogen were compared to existing experimental data for normal hydrogen. The comparison of predicted and experimental vapor pressures from the new normal hydrogen EOS is shown in Fig. 24. The most recent vapor-pressure measurements of normal hydrogen are those of Hiza.⁴⁷ The majority of the data in this set are within 0.2% of the predicted data, indicating that above 20 K the transformed data are in agreement with the existing experimental data. Below 20 K, however, there is little agreement among existing experimental data sets. The transformed data agree within 0.3% with the primary data set of Scott *et al.*⁷⁷

The single-phase density data of Goodwin *et al.*⁴¹ and Roder *et al.*⁷³ were selected for transformation to the normal hydrogen and orthohydrogen surfaces of state due to the accuracy and precision of the data. No data above 60 K were transformed to prevent excessive errors from the quantum

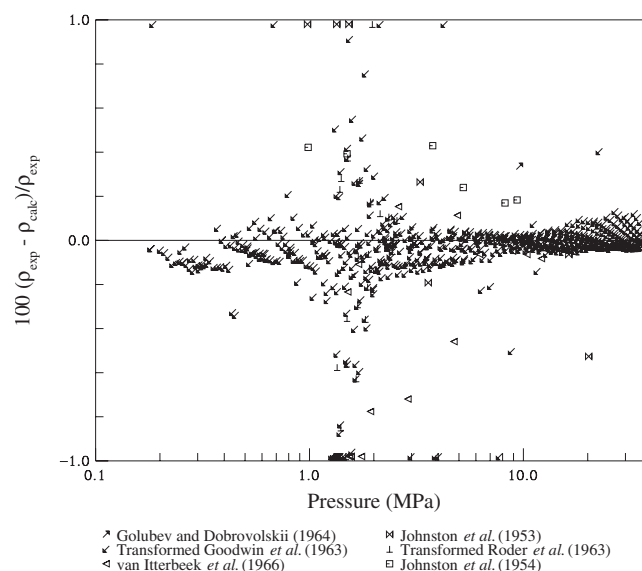


FIG. 25. Comparison of calculated densities for the new normal hydrogen EOS to experimental and predicted data.

parameters being based on the ground-state intermolecular potentials. Due to the large size of the original data sets, selected points from these transformations are shown in Table 11. The deviations of predicted and experimental data in the 14–40 K region from the new normal hydrogen EOS are shown in Fig. 25.

There are four experimental data sets in the 14–40 K region for comparison with the predicted data. The data sets of van Itterbeek *et al.*⁸⁵ and Johnston *et al.*^{54,55} show differing trends near the normal hydrogen critical pressure of 1.2964 MPa. The predicted data are unable to resolve this discrepancy; however, the predicted data lie within the uncertainty of the existing experimental data sets. No set of predicted orthohydrogen data was compared with experimental data because no experimental orthohydrogen data exist.¹

6.3. Comparison of Calculated Normal Hydrogen Data to Experimental Data

Table 12 lists the available normal hydrogen experimental data. Some of the data published prior to 1933 were taken

TABLE 11. Selected parahydrogen single-phase density data and the data transformed to the normal hydrogen and orthohydrogen surfaces of state

Author	Parahydrogen (original)			Normal hydrogen			Orthohydrogen		
	<i>T</i> (K)	<i>p</i> (MPa)	ρ (mol dm ⁻³)	<i>T</i> (K)	<i>p</i> (MPa)	ρ (mol dm ⁻³)	<i>T</i> (K)	<i>p</i> (MPa)	ρ (mol dm ⁻³)
Goodwin <i>et al.</i> ⁴¹	31.995	0.2567	1.084	32.187	0.2681	1.084	32.201	0.2683	1.084
Goodwin <i>et al.</i> ⁴¹	29.997	0.8742	26.962	30.178	0.8808	26.962	30.191	0.8816	26.962
Goodwin <i>et al.</i> ⁴¹	18.993	18.158	42.111	19.114	18.294	42.111	19.130	18.309	42.111
Roder <i>et al.</i> ⁷³	32.995	1.2977	16.398	33.193	1.3074	16.398	33.207	1.3085	16.398
Roder <i>et al.</i> ⁷³	33.195	1.3311	14.098	33.394	1.3411	14.098	33.408	1.3422	14.098
Roder <i>et al.</i> ⁷³	37.997	2.2354	15.116	38.223	2.2521	15.116	38.236	2.2540	15.116

TABLE 12. Normal hydrogen experimental data and AAD from the new and Younglove⁷ EOS

Reference	Rank	Total points	<i>T</i> (K)	<i>p</i> (MPa)	AAD from new EOS	AAD from Younglove
<i>p</i> - <i>ρ</i> - <i>T</i>						
Amagat (1893) ²⁵	2	73	273.2–320.4	0.1–304.0	0.38	0.44
Bartlett (1927) ²⁹	2	8	273.2	5.1–101.3	0.32	0.37
Bartlett <i>et al.</i> (1928) ³⁰	2	43	273.2–673.0	5.1–101.3	0.27	0.29
Bartlett <i>et al.</i> (1930) ³¹	2	54	203–293	2.6–102.7	0.47	0.38
David and Hamann (1953) ³⁶	2	12	65–79	30.4–126.7	0.83	0.53
Holborn and Otto (1925) ⁵¹	2	30	65.25–223.1	2.0–10.0	0.12	0.17
Jaeschke and Humphreys						
Gasunie (1990) ⁵²	1	68	273.2–353	0.2–26.3	0.01	0.04
Ruhrgas (1990) ⁵²	1	221	273.2–353	0.5–28.1	0.01	0.04
Johnston <i>et al.</i> (1953) ⁵⁵	2	227	33–300	0.5–20.6	0.48	0.69
Liebenberg <i>et al.</i> (1978) ⁵⁹	1	19	75.0–163.9	473–1871	8.58	– ^a
Liebenberg <i>et al.</i> (1977) ⁶⁰	1	1953	75–307	200–2000	1.41	4.78
Machado <i>et al.</i> (1988) ⁶³	2	60	130–159	1.2–105.5	3.73	5.16
Michels and Goudekot (1941) ⁶⁷	2	283	273–423	0.9–300.9	0.09	0.13
Michels <i>et al.</i> (1959) ⁶⁵	1	482	98.2–423.2	0.7–299.2	0.06	0.11
Presnall (1969) ⁷²	1	108	473.1–873.0	10.1–182.4	1.19	1.34
Scott (1929) ⁷⁶	2	18	298	0.1–17.2	0.09	0.14
Townend and Bhatt (1931) ⁸⁰	2	40	273–298	0.1–60.8	0.16	0.11
van Itterbeek <i>et al.</i> (1966) ⁸⁵	2	161	21.2–40.7	0.3–16.1	1.27	1.25
Verschoye (1926) ⁸⁸	2	25	273–293	5.0–21.0	0.11	0.15
Wiebe and Gaddy (1938) ⁹²	2	47	273–573	2.5–101.3	0.09	0.08
Vapor pressure						
Aston <i>et al.</i> (1935) ²⁶	2	4	18.0–20.7	sat	1.74	4.65
Barber (1964) ²⁷	2	1	13.816	sat	3.02	3.02
Grilly (1951) ⁴³	2	8	19.3–24.5	sat	1.68	3.53
Henning (1926) ⁴⁵	2	25	14.0–20.5	sat	3.20	6.78
Henning and Otto (1936) ⁴⁶	2	19	13.93–20.38	sat	10.49	13.11
Hiza (1981) ⁴⁷	1	12	20.0–30.0	sat	0.17	2.40
Keesom <i>et al.</i> (1931) ⁵⁶	2	31	17.2–20.5	sat	1.38	4.25
Scott (1934) ⁷⁷	1	10	15.2–20.3	sat	0.40	2.86
Traver <i>et al.</i> (1902) ⁸¹	2	9	14.9–20.4	sat	6.48	3.53
van Itterbeek <i>et al.</i> (1964) ⁸⁶	2	42	20.6–32.3	sat	2.10	3.54
White (1950) ⁹⁰	2	17	20.9–33.1	sat	1.59	3.79
White (1950) ⁹¹	2	6	33.08–33.25	sat	1.23	3.33
Speed of sound						
Guesewell <i>et al.</i> (1970) ⁴⁴	1	7	25–31	0.1	0.55	6.37
Liebenberg <i>et al.</i> (1978) ⁵⁹	2	19	75.0–163.9	473–1871	11.96	– ^a
Liebenberg <i>et al.</i> (1977) ⁶⁰	2	1953	75–307	200–2000	4.14	12.33
van Dael <i>et al.</i> (1965) ²³	1	175	22.2–33	0.2–24.8	0.60	1.82
van Itterbeek <i>et al.</i> (1961) ⁸⁴	1	42	14.1–20.4	0.009–0.1	0.32	1.69
van Itterbeek <i>et al.</i> (1963) ⁸³	1	110	15.1–20.5	0.02–23.5	0.25	6.37
Second virial coefficient						
Bartlett <i>et al.</i> (1928) ³⁰	2	5	273.2–572.3	–	0.69	0.52
Beenakker <i>et al.</i> (1959) ³²	2	1	20.4	–	9.56	10.02
Cottrell <i>et al.</i> (1956) ³⁵	2	1	303.2	–	0.54	1.04
Dehaas (1912) ³⁷	2	3	289.1–293.7	–	16.85	15.99
El Hadi <i>et al.</i> (1969) ³⁸	2	7	19.3–26.3	–	1.49	1.48
Gibby <i>et al.</i> (1929) ³⁹	2	7	298.2–448.2	–	0.24	0.48
Holborn and Otto (1925) ⁵¹	2	8	90.2–473.2	–	3.48	3.05
Holborn and Otto (1926) ⁵⁰	2	9	65.3–473.2	–	10.63	11.12
Johnston <i>et al.</i> (1953) ⁵⁵	2	18	35.1–300	–	0.86	0.20
Kerl (1982) ⁵⁷	2	1	293.1	–	–	– ^b
Knaap <i>et al.</i> (1962) ⁵⁸	2	23	20.5–65.0	–	7.22	5.69
Long and Brown (1937) ⁶¹	2	7	20.9–46.5	–	1.3	1.83

TABLE 12. Normal hydrogen experimental data and AAD from the new and Younglove⁷ EOS—Continued

Reference	Rank	Total points	T (K)	p (MPa)	AAD from new EOS	AAD from Younglove
Lopatinskii <i>et al.</i> (1991) ⁶²	2	2	293.2	—	0.96	0.43
Michels and Goudekert (1941) ⁶⁷	2	20	273.2–423.2	—	0.75	1.14
Michels <i>et al.</i> (1959) ⁶⁵	2	17	98.2–423.2	—	0.35	0.77
Michels <i>et al.</i> (1960) ⁶⁶	1	17	98.2–423.2	—	4.87	5.03
Mihara <i>et al.</i> (1977) ⁶⁸	2	3	298.2–348.2	—	0.22	0.57
Mueller <i>et al.</i> (1961) ⁶⁹	2	6	73.2–323.2	—	8.21	8.85
Nijhoff and Keesom (1927) ⁷⁰	2	8	24.8–373.2	—	0.84	1.54
Perez <i>et al.</i> (1980) ⁷¹	2	5	300–500	—	0.49	0.75
Schramm <i>et al.</i> (1991) ⁷⁵	2	1	296.2	—	0.40	0.92
Scott (1929) ⁷⁶	2	1	298.2	—	0.06	0.45
Townend and Bhatt (1931) ⁸⁰	2	2	273.2–298.2	—	0.63	0.59
van Agt and Onnes (1925) ⁸²	2	9	14.6–90.3	—	5.93	3.90
Varekamp and Beenakker (1959) ⁸⁷	2	8	14.0–21.0	—	12.01	8.87
Verschoye (1926) ⁸⁸	2	2	273.2–293.2	—	0.11	0.44
Wiebe and Gaddy (1938) ⁹²	2	6	273.2–573.2	—	0.51	0.39
Third virial coefficient						
Holborn and Otto (1925) ⁵¹	2	5	90.2–273.2	—	1.04	0.99
Johnston <i>et al.</i> (1953) ⁵⁵	2	18	35.1–300.0	—	0.28	0.11
Michels and Goudekert (1941) ⁶⁷	2	20	273.2–423.2	—	0.48	0.53
Michels <i>et al.</i> (1959) ⁶⁵	2	17	98.2–423.2	—	0.13	0.14
Michels <i>et al.</i> (1960) ⁶⁶	1	17	98.2–423.2	—	0.09	0.15
Mihara <i>et al.</i> (1977) ⁶⁸	2	3	298.2–348.2	—	0.08	0.12
Scott (1929) ⁷⁶	2	1	298.2	—	0.26	0.20
Townend and Bhatt (1931) ⁸⁰	2	2	273.2–298.2	—	0.19	0.12
Verschoye (1926) ⁸⁸	2	2	273.2–293.2	—	0.03	0.03

^aThese data could not be compared because the Younglove (Ref. 7) EOS behaves unphysically at very high densities.

^bDiscrepancies between this data set and other experimental data could not be resolved, so no comparison is given.

before the existence of orthohydrogen and parahydrogen was established¹² and are compared to normal hydrogen here, although the true concentration of the measured samples is uncertain.

Figures 26 and 27 compare calculated virial coefficients with experimental data. No virial-coefficient data were used in the regression, so their representation is based on agreement with p - ρ - T data.

No experimental data for saturation heat capacity, isochoric heat capacity, or isobaric heat capacity exist that are suitable for correlation. Figure 28 compares calculated vapor pressures with experimental normal hydrogen data. The data of Hiza⁴⁷ are the most recent available. Vapor pressures were calculated from the new parahydrogen EOS and transformed to the normal hydrogen surface using the procedure discussed previously. The data of Scott⁷⁷ were chosen as primary below the normal boiling point because the data appear to trend well with experimental vapor-pressure data at higher temperatures, and the transformed vapor pressures of the new parahydrogen EOS.

Speed-of-sound comparisons for both the new and Younglove⁷ normal hydrogen equations of state are shown in Fig. 29. The data set of Güsewell *et al.*⁴⁴ is the most recent and was chosen as primary. As with parahydrogen, speed-of-sound values near the critical pressure exhibit significant de-

viations, possibly because of the lack of critical-region terms in the equations of state that could aid the speed of sound to approach zero at the critical point.

Figures 30–35 display deviations of densities plotted versus pressure, separated into increments of temperature, as noted in the upper right corner of each graph. In most of the plots, the new EOS displays significant improvements over the Younglove⁷ normal hydrogen EOS. The QLCS was used to transform the single-phase data of Goodwin *et al.*⁴¹ and Roder *et al.*⁷³ to the normal hydrogen surface of state; once transformed, the data agreed fairly well with those of Johnston *et al.*⁵⁵ The deviations of density from the transformed data are included in Figs. 25, 36, and 37. The original data of Goodwin *et al.*⁴¹ and Roder *et al.*⁷³ are included in the figures to illustrate the similarities between the normal hydrogen and parahydrogen surfaces of state. At pressures over 20 MPa, the deviations between the original and transformed data become small. Figures 36 and 37 display all of the density data on a single plot to show that the new normal hydrogen EOS reproduces the high-pressure data of Liebenberg *et al.*^{59,60} The representation of the high-temperature data of Presnall⁷² could not be improved because all attempts to do so created discrepancies with the primary data of Michels *et al.*⁶⁵ Figure 36 displays solid bars of data over 300 MPa; these data from Liebenberg *et al.*^{59,60} could not be

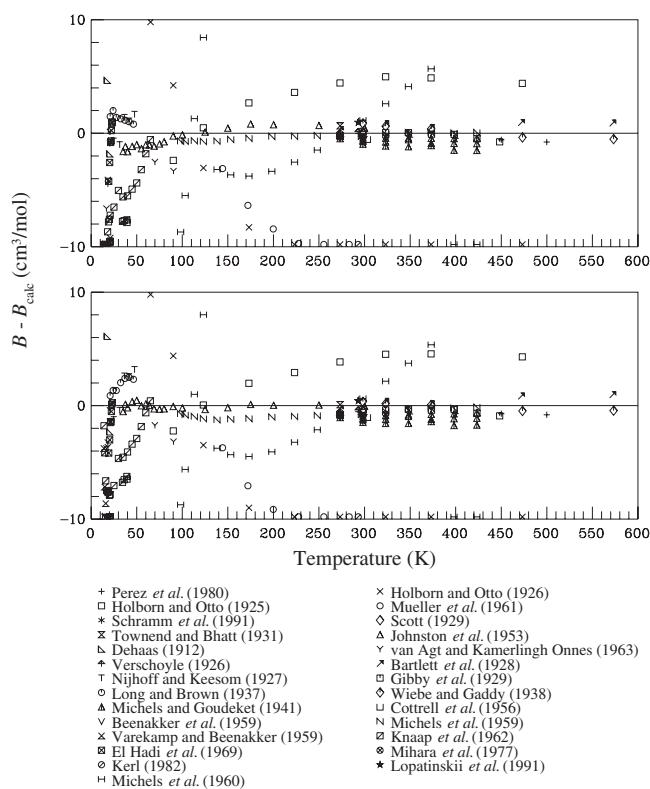


Fig. 26. Comparison of calculated second virial coefficients plotted versus temperature for the new normal hydrogen EOS (top) and the normal hydrogen EOS of Younglove (bottom) to experimental data.

compared to the Younglove⁷ EOS because of the physical behavior of the isotherms predicted by the EOS in this particular region of the surface of state.

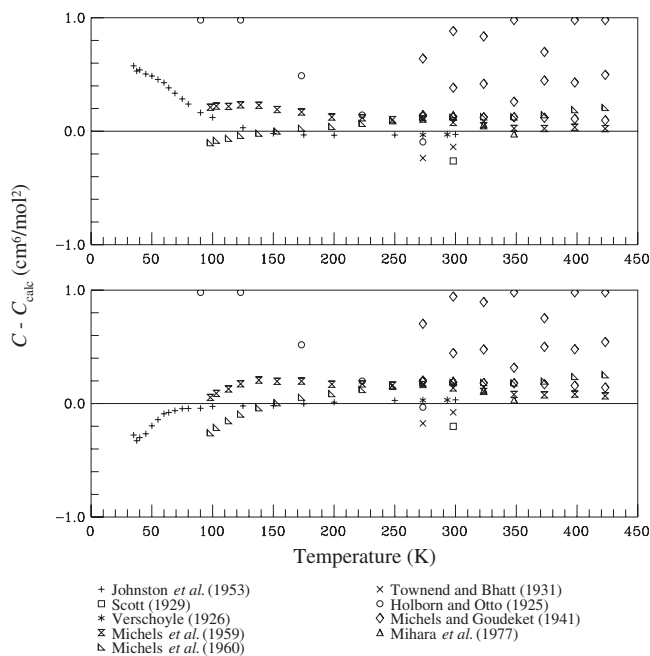


Fig. 27. Comparison of calculated third virial coefficients plotted versus temperature for the new normal hydrogen EOS (top) and the normal hydrogen EOS of Younglove (bottom) to experimental data.

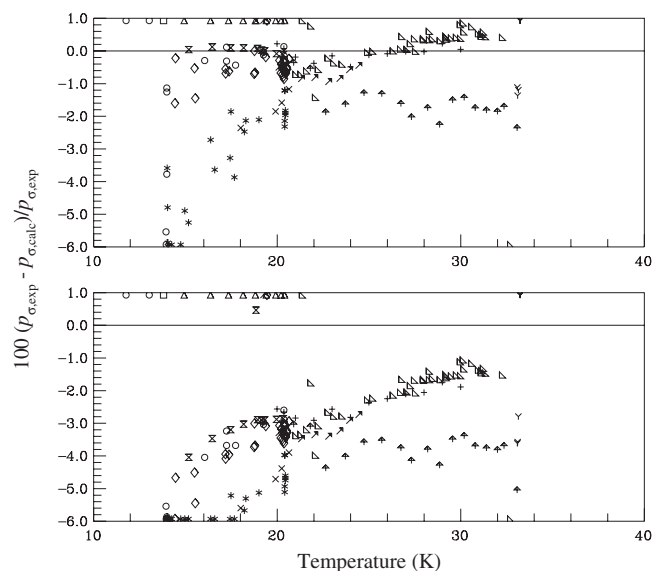


Fig. 28. Comparison of calculated vapor pressures plotted versus temperature for the new normal hydrogen EOS (top) and the normal hydrogen EOS of Younglove (bottom) to experimental data and transformed data.

6.4. Comparison of Calculated Orthohydrogen Data to Transformed Experimental Data

In this section all comparisons are made to data predicted by use of the QLCS where the deviations between normal hydrogen data and orthohydrogen data are large enough to warrant the use of predictions. Where the differences between the densities of orthohydrogen and normal hydrogen

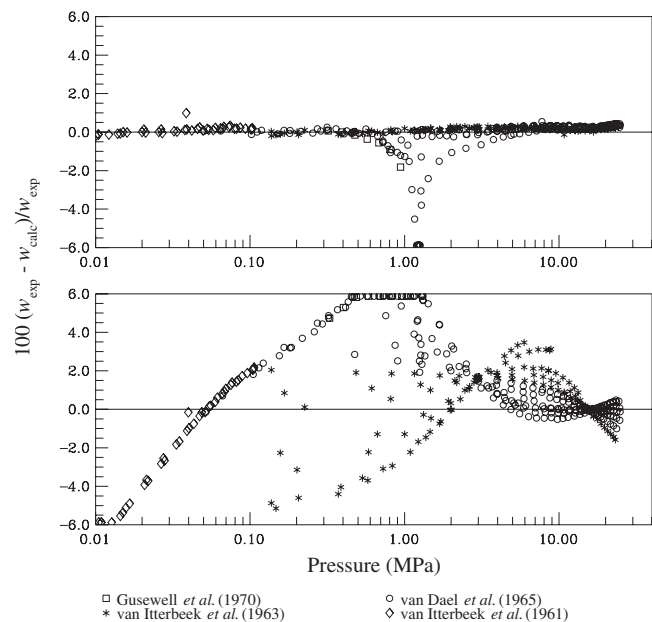


Fig. 29. Comparison of calculated sound speeds plotted versus pressure for the new normal hydrogen EOS (top) and the normal hydrogen EOS of Younglove (bottom) to experimental data.

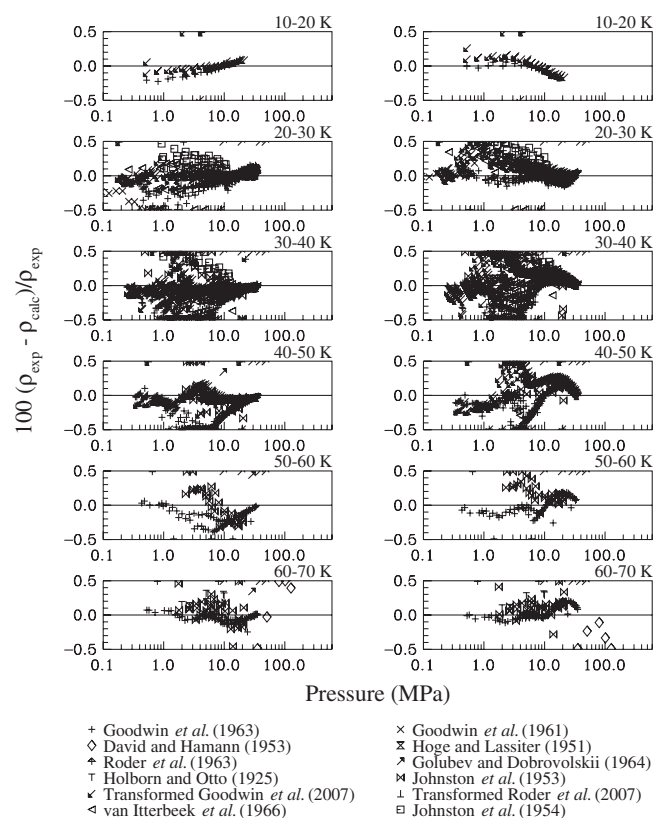


FIG. 30. Comparison of calculated densities plotted versus pressure for the new normal hydrogen EOS (left) and the normal hydrogen EOS of Younglove (right) to experimental data (data plotted in 10 K increments from 10 to 80 K).

are smaller than the experimental uncertainty of the available normal hydrogen data, the original normal hydrogen density data were also included in the density and pressure deviation plots. Vapor-pressure, speed-of-sound, and density data were verified as accurate during the transformation process, and these data were the only data used in the regression and shown in the comparisons.

Figure 38 shows deviations of calculated vapor pressures from predicted data. The normal hydrogen vapor-pressure data are included in this plot to illustrate the differences between vapor pressures of orthohydrogen and normal hydrogen. These values were calculated with the new parahydrogen EOS and transformed to the orthohydrogen surface.

Speed-of-sound comparisons for the new orthohydrogen EOS are shown in Figure 39. The normal hydrogen data sets of van Isterbeek *et al.*^{83,84} and van Dael *et al.*²³ were chosen as primary for transformation to the orthohydrogen surface.

Figures 40–42 display deviations of densities plotted versus pressure and are separated into increments of temperature, as shown in the upper right corner of each graph. The QLCS was used to transform the single-phase data of Goodwin *et al.*⁴¹ and Roder *et al.*⁷³ to the orthohydrogen surface of state. The original Goodwin *et al.*⁴¹ and Roder *et al.*⁷³ parahydrogen data are included in the figures to display similarities between the surfaces of state for orthohydrogen and parahydrogen. At pressures over 20 MPa, the deviations between original and transformed data become small.

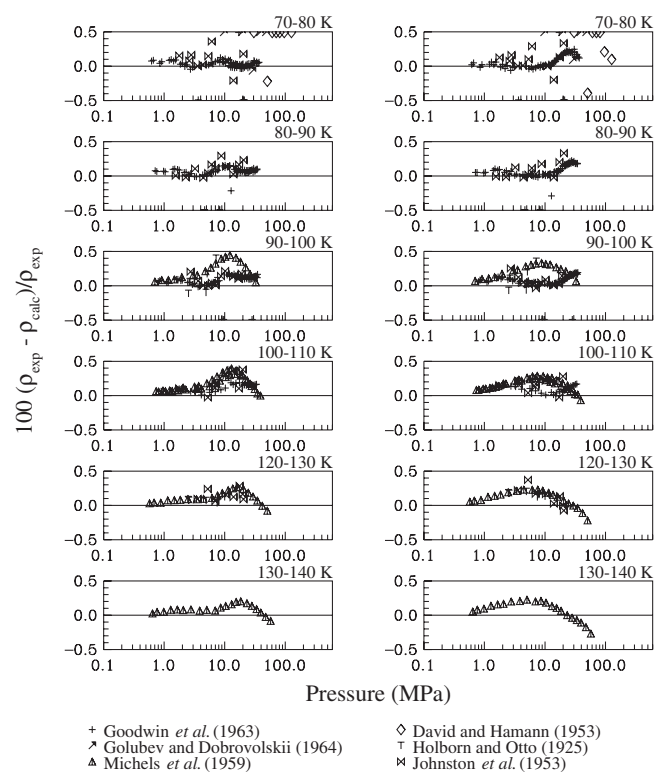


FIG. 31. Comparison of calculated densities plotted versus pressure for the new normal hydrogen EOS (left) and the normal hydrogen EOS of Younglove (right) to experimental data (data plotted in 10 K increments from 70 to 140 K).

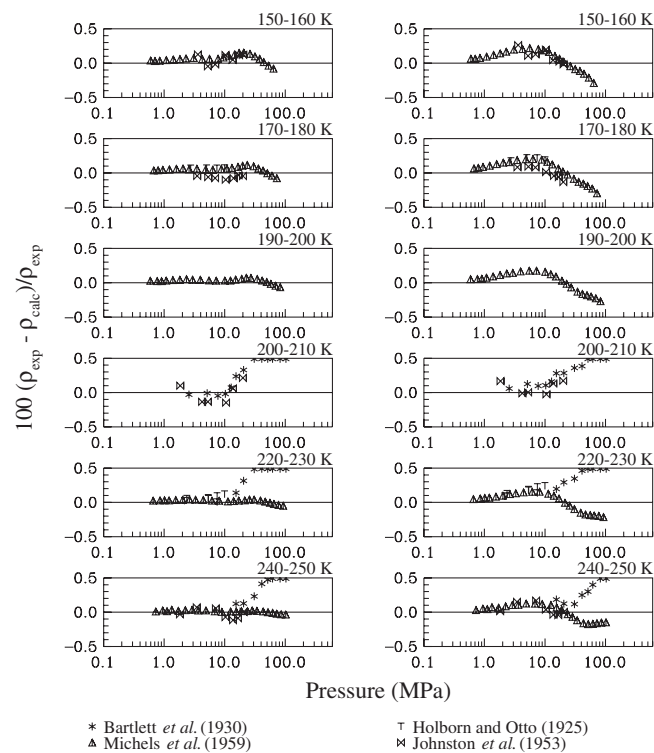


FIG. 32. Comparison of calculated densities plotted versus pressure for the new normal hydrogen EOS (left) and the normal hydrogen EOS of Younglove (right) to experimental data (data plotted in 10 K increments from 150 to 250 K).

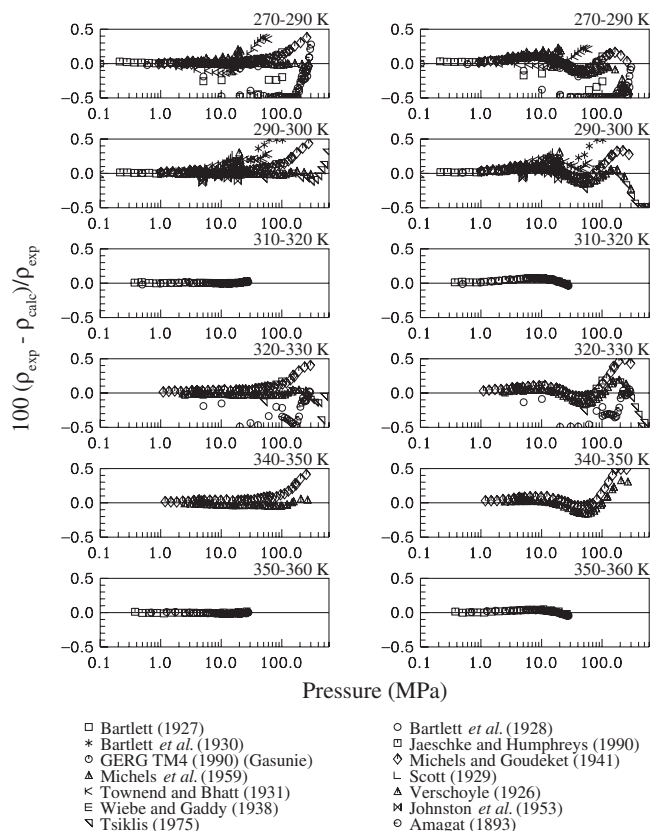


FIG. 33. Comparison of calculated densities plotted versus pressure for the new normal hydrogen EOS (left) and the normal hydrogen EOS of Younglove (right) to experimental data (data plotted in 10 K increments from 270 to 360 K).

7. Results and Recommendations for Future Research

Three new fundamental equations of state for parahydrogen, normal hydrogen, and orthohydrogen have been devel-

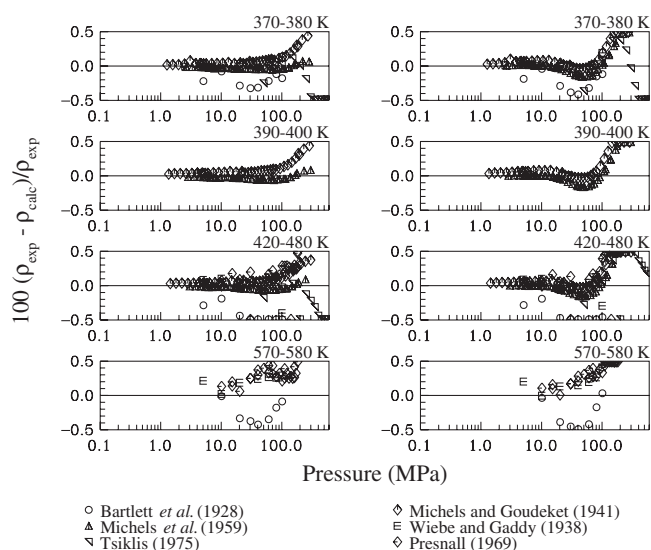


FIG. 34. Comparison of calculated densities plotted versus pressure for the new normal hydrogen EOS (left) and the normal hydrogen EOS of Younglove (right) to experimental data (data plotted in listed increments from 370 to 580 K).

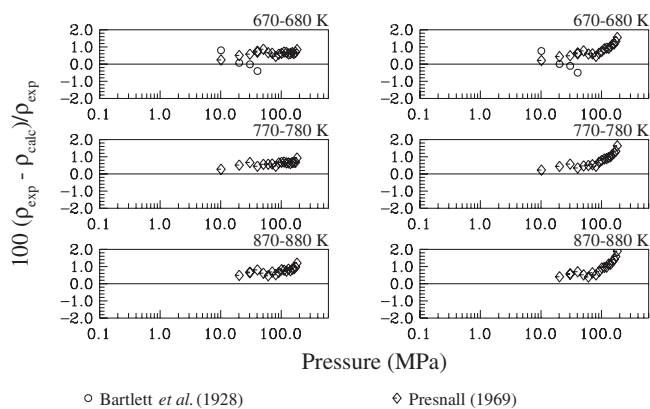


FIG. 35. Comparison of calculated densities plotted versus pressure for the new normal hydrogen EOS (left) and the normal hydrogen EOS of Younglove (right) to experimental data (data plotted in listed increments from 670 to 880 K).

oped. The equations represent the available experimental data to within the estimated uncertainty of the data. The formulations extend the existing ranges of reliable property predictions to 2000 MPa and 1000 K and improve the uncertainty in predicted properties. The formulations predict different caloric and near-critical region properties for parahydrogen, orthohydrogen, and the 3:1 mixture treated here as a pure fluid, normal hydrogen.

The estimated combined expanded uncertainty with a coverage factor of 2 for primary data sets in density of the EOS for parahydrogen is 0.1% at temperatures from the triple

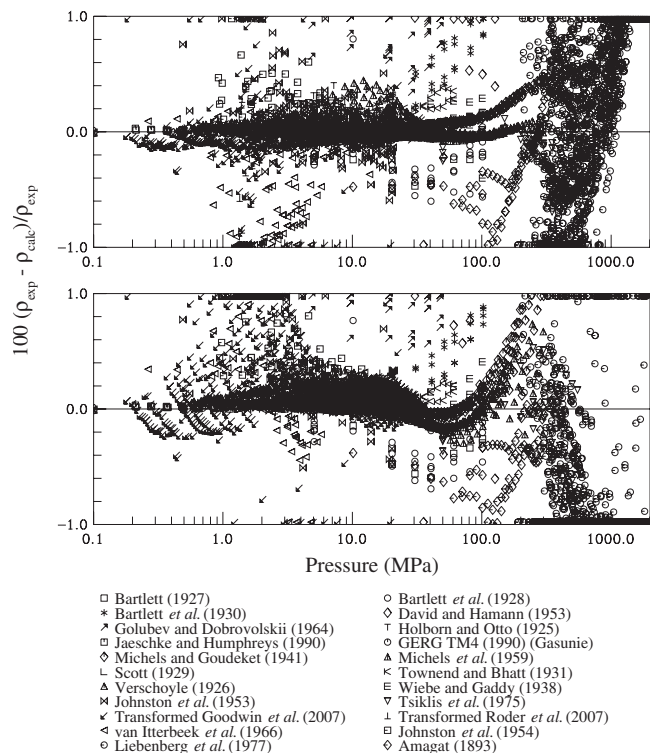


FIG. 36. Comparison of calculated densities plotted versus pressure for the new normal hydrogen EOS (top) and the normal hydrogen EOS of Younglove (bottom) to experimental data.

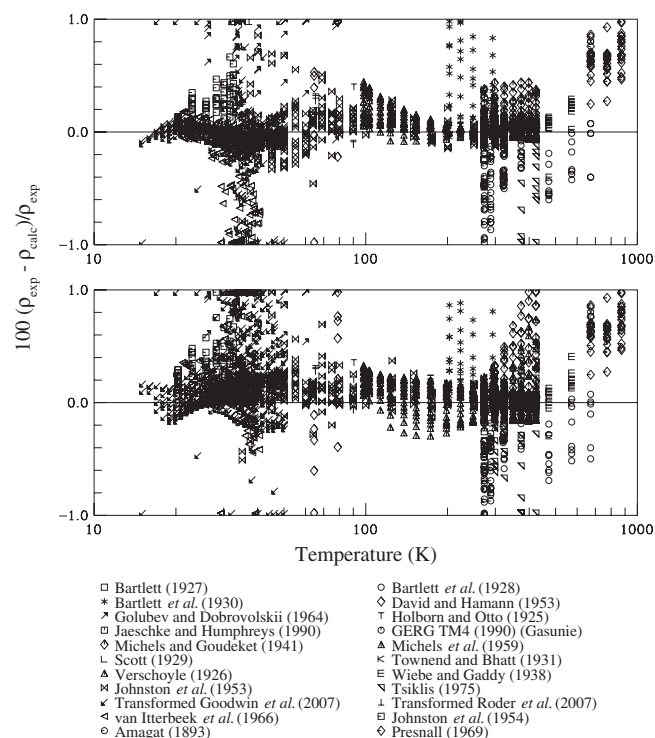


Fig. 37. Comparison of calculated densities plotted versus temperature for the new normal hydrogen EOS (top) and the normal hydrogen EOS of Younglove (bottom) to experimental data.

point to 250 K and at pressures up to 40 MPa, except in the critical region, where an uncertainty of 0.2% in pressure is generally observed. In the region between 250 and 450 K and at pressures up to 300 MPa, the uncertainty in density is 0.04%. At temperatures between 450 and 1000 K, the uncertainty in density increases to 1%. Uncertainties of calculated

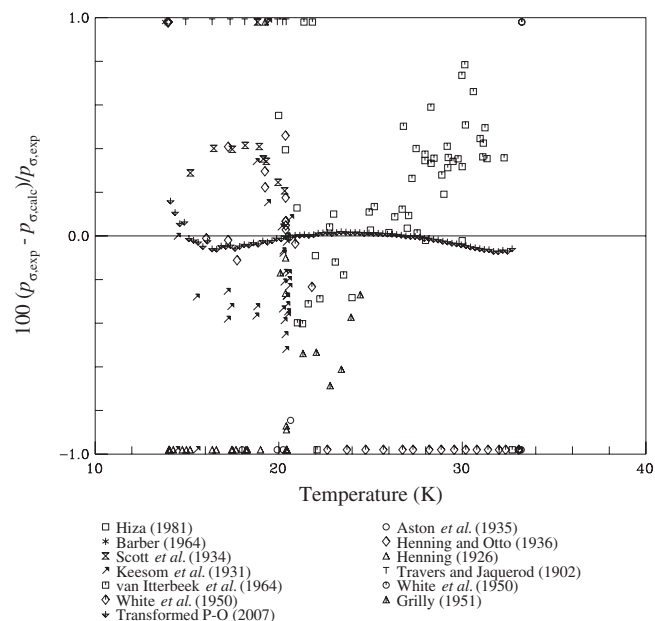


Fig. 38. Comparison of calculated vapor pressures plotted versus temperature for the new orthohydrogen EOS to experimental and predicted data.

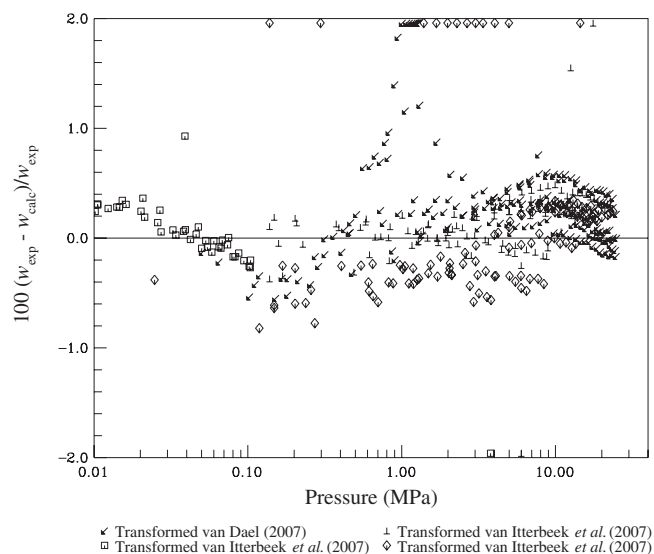


Fig. 39. Comparison of calculated sound speeds plotted versus pressure for the new orthohydrogen EOS to predicted data.

densities at pressures above 300 MPa increase from 0.04% to a maximum of 1% near the extreme of 2000 MPa. Speed-of-sound data are represented to within 0.5% below 100 MPa. The estimated uncertainty for heat capacities is 1.0%. The estimated uncertainties of vapor pressures and saturated liquid densities calculated using the Maxwell criterion are 0.1% for each property.

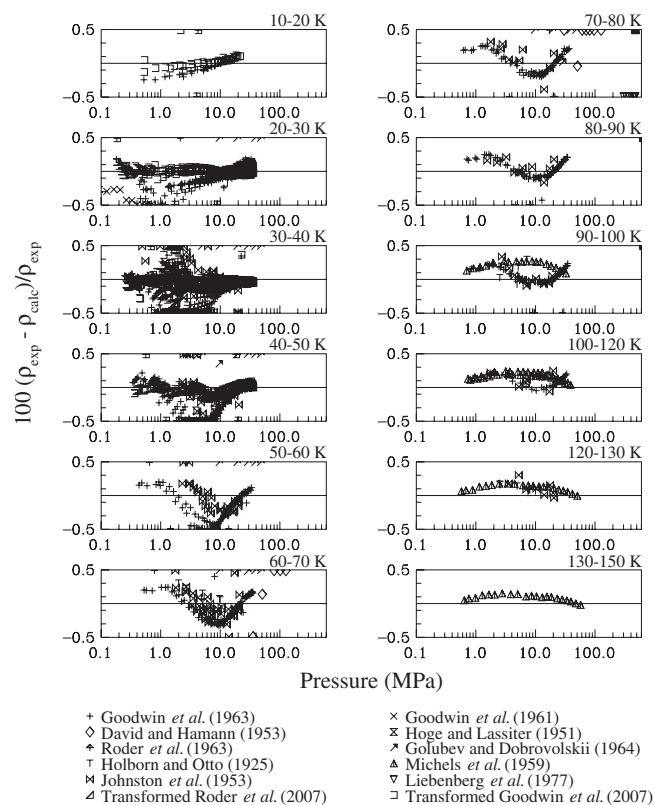


Fig. 40. Comparison of calculated densities plotted versus pressure for the new orthohydrogen EOS to experimental and predicted data (data shown in increments from 10 to 150 K).

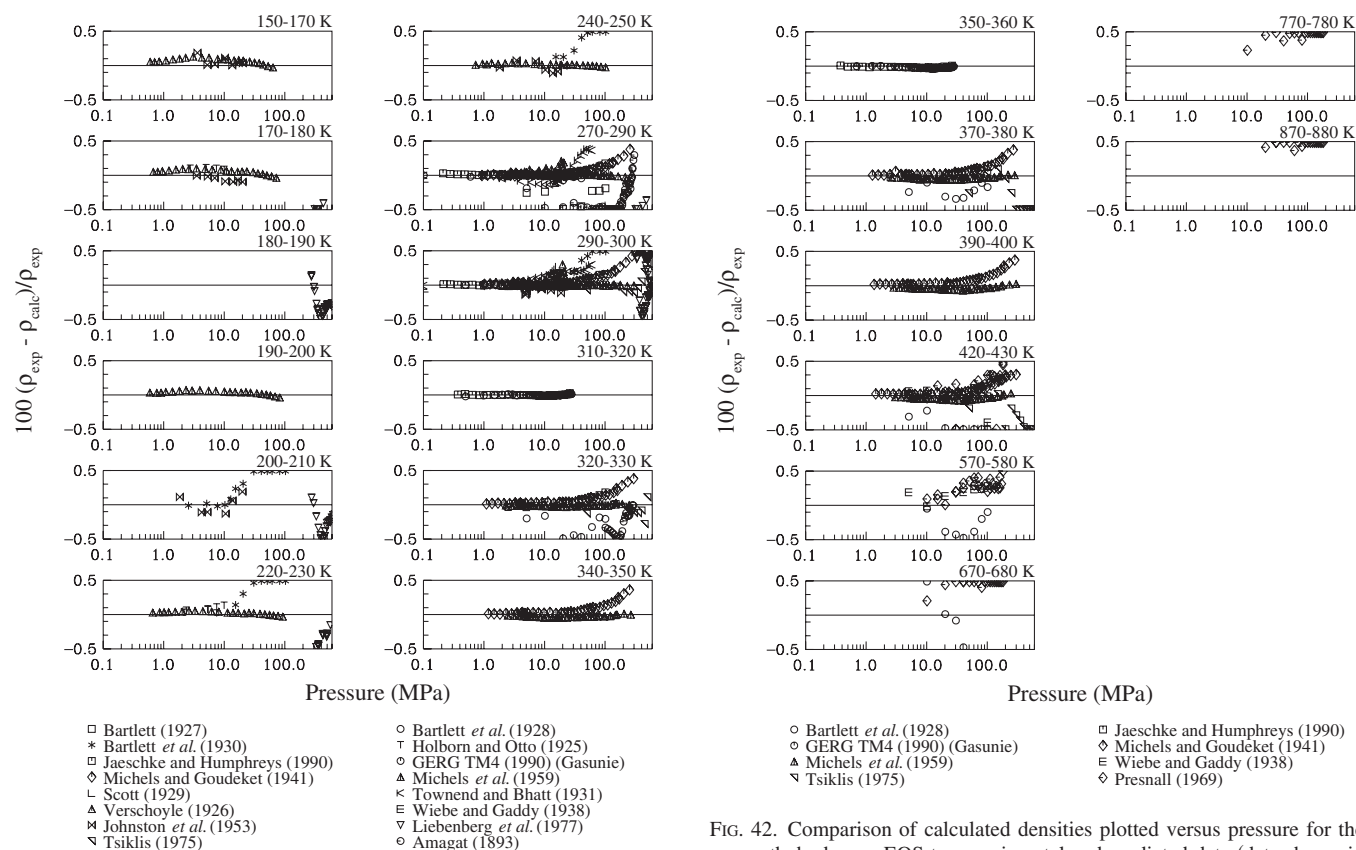


Fig. 41. Comparison of calculated densities plotted versus pressure for the new orthohydrogen EOS to experimental and predicted data (data shown in increments from 150 to 350 K).

Fig. 42. Comparison of calculated densities plotted versus pressure for the new orthohydrogen EOS to experimental and predicted data (data shown in increments from 350 to 880 K).

TABLE 13. Tabulated thermodynamic properties of parahydrogen at saturation

<i>T</i> (K)	<i>p</i> (kPa)	Liquid ρ (kg/m ³)	Vapor ρ (kg/m ³)	Liquid <i>h</i> (kJ/kg)	Vapor <i>h</i> (kJ/kg)	Liquid <i>s</i> (kJ/kg K)	Vapor <i>s</i> (kJ/kg K)	Liquid <i>c_v</i> (kJ/kg K)	Vapor <i>c_v</i> (kJ/kg K)	Liquid <i>c_p</i> (kJ/kg K)	Vapor <i>c_p</i> (kJ/kg K)	Liquid <i>w</i> (m/s)	Vapor <i>w</i> (m/s)
13.8033	7.0410	76.977	0.125 55	-53.741	396.31	-3.084 0	29.521	5.1313	6.2265	6.9241	10.534	1263.1	305.65
14	7.8840	76.819	0.138 78	-52.364	398.14	-2.985 7	29.193	5.1576	6.2358	6.9807	10.559	1256.9	307.56
15	13.434	75.996	0.222 40	-45.167	407.19	-2.494 3	27.663	5.2616	6.2818	7.2990	10.703	1231.3	316.84
16	21.548	75.133	0.337 66	-37.603	415.83	-2.013 2	26.326	5.3343	6.3225	7.6586	10.869	1210.4	325.43
17	32.886	74.220	0.490 69	-29.626	423.97	-1.538 9	25.143	5.4003	6.3569	8.0621	11.063	1190.1	333.39
18	48.148	73.252	0.688 00	-21.184	431.52	-1.068 4	24.082	5.4720	6.3870	8.5133	11.294	1168.5	340.72
19	68.071	72.225	0.936 56	-12.224	438.41	-0.598 83	23.119	5.5516	6.4167	9.0145	11.574	1144.7	347.43
20	93.414	71.135	1.244 0	-2.691 5	444.54	-0.128 14	22.234	5.6371	6.4499	9.5688	11.920	1118.6	353.50
20.271	101.325	70.828	1.338 5	-0.002 51	446.06	-0.000 12	22.005	5.6608	6.4599	9.7288	12.028	1111.1	355.04
21	124.960	69.977	1.618 8	7.468 9	449.84	0.345 67	21.411	5.7248	6.4902	10.182	12.349	1090.1	358.94
22	163.500	68.743	2.070 8	18.318	454.20	0.824 41	20.637	5.8115	6.5406	10.865	12.884	1059.2	363.71
23	209.830	67.425	2.611 4	29.925	457.53	1.310 0	19.902	5.8949	6.6036	11.635	13.553	1025.9	367.83
24	264.780	66.010	3.254 6	42.371	459.71	1.804 5	19.194	5.9739	6.6814	12.520	14.398	989.95	371.27
25	329.170	64.485	4.017 8	55.761	460.61	2.310 7	18.505	6.0485	6.7759	13.561	15.480	951.23	374.03
26	403.840	62.827	4.923 6	70.230	460.03	2.832 1	17.824	6.1200	6.8895	14.827	16.898	909.32	376.10
27	489.650	61.006	6.002 9	85.961	457.73	3.373 3	17.143	6.1908	7.0254	16.429	18.814	863.64	377.48
28	587.500	58.980	7.299 8	103.22	453.35	3.941 4	16.446	6.2660	7.1879	18.569	21.525	813.34	378.15
29	698.330	56.677	8.883 0	122.41	446.33	4.547 5	15.717	6.3541	7.3840	21.653	25.636	757.14	378.08
30	823.190	53.976	10.871	144.24	435.71	5.210 8	14.926	6.4715	7.6246	26.649	32.583	693.04	377.20
31	963.290	50.626	13.508	170.13	419.51	5.971 3	14.016	6.6543	7.9291	36.573	46.818	617.45	375.35
32	1120.300	45.901	17.492	204.08	392.26	6.945 2	12.826	7.0097	8.3364	68.189	92.392	522.59	372.03
32.938	1285.800	31.323	31.323	295.63	295.63	9.625 3	9.6253	-	-	-	-	-	-

TABLE 14. Tabulated thermodynamic properties of normal hydrogen at saturation

T (K)	p (kPa)	Liquid ρ (kg/m ³)	Vapor ρ (kg/m ³)	Liquid h (kJ/kg)	Vapor h (kJ/kg)	Liquid s (kJ/kg K)	Vapor s (kJ/kg K)	Liquid c_v (kJ/kg K)	Vapor c_v (kJ/kg K)	Liquid c_p (kJ/kg K)	Vapor c_p (kJ/kg K)	Liquid w (m/s)	Vapor w (m/s)
13.957	7.3580	77.004	0.129 85	-53.926	399.83	-3.072 3	29.438	5.1616	6.2433	7.0212	10.564	1269.2	307.14
14	7.5410	76.969	0.132 72	-53.622	400.22	-3.050 7	29.367	5.1625	6.2449	7.0312	10.570	1268.3	307.56
15	12.898	76.136	0.213 46	-46.388	409.28	-2.556 6	27.821	5.2313	6.2814	7.3386	10.703	1247.1	316.97
16	20.755	75.264	0.325 06	-38.777	417.91	-2.072 2	26.471	5.3287	6.3140	7.7212	10.860	1225.5	325.71
17	31.759	74.345	0.473 56	-30.733	426.05	-1.593 6	25.276	5.4192	6.3427	8.1368	11.047	1203.4	333.81
18	46.602	73.375	0.665 27	-22.224	433.60	-1.118 8	24.204	5.4986	6.3701	8.5793	11.274	1180.2	341.28
19	66.006	72.350	0.906 93	-13.215	440.49	-0.646 25	23.233	5.5700	6.3996	9.0539	11.551	1155.5	348.12
20	90.717	71.265	1.205 9	-3.667 2	446.64	-0.174 29	22.341	5.6369	6.4343	9.5697	11.892	1129.1	354.31
20.369	101.325	70.848	1.332 2	0.000 97	448.71	4.56E-05	22.029	5.6609	6.4490	9.7725	12.037	1118.9	356.42
21	121.500	70.115	1.570 1	6.466 0	451.98	0.298 76	21.514	5.7015	6.4768	10.138	12.312	1100.8	359.84
22	159.130	68.893	2.009 0	17.241	456.43	0.774 72	20.738	5.7649	6.5292	10.771	12.830	1070.3	364.70
23	204.380	67.592	2.533 4	28.724	459.88	1.255 6	20.002	5.8276	6.5927	11.490	13.472	1037.5	368.88
24	258.070	66.199	3.156 2	40.997	462.24	1.743 7	19.296	5.8898	6.6685	12.319	14.273	1002.2	372.38
25	321.000	64.701	3.893 8	54.161	463.37	2.241 7	18.610	5.9521	6.7578	13.298	15.289	964.22	375.20
26	393.990	63.079	4.767 4	68.346	463.10	2.753 1	17.936	6.0155	6.8620	14.487	16.603	923.11	377.33
27	477.890	61.305	5.805 5	83.727	461.18	3.282 5	17.262	6.0820	6.9832	15.987	18.357	878.38	378.77
28	573.590	59.339	7.048 9	100.55	457.30	3.836 5	16.577	6.1552	7.1248	17.977	20.804	829.30	379.55
29	682.050	57.119	8.560 1	119.20	450.92	4.425 3	15.864	6.2415	7.2922	20.807	24.445	774.76	379.64
30	804.320	54.538	10.445	140.30	441.19	5.066 1	15.096	6.3535	7.4945	25.284	30.425	713.07	379.07
31	941.650	51.381	12.909	165.08	426.41	5.793 3	14.223	6.5181	7.7475	33.759	42.069	641.21	377.80
32	1095.700	47.085	16.495	196.73	402.30	6.698 3	13.122	6.8110	8.0826	57.287	74.636	552.88	375.78
33	1269.300	38.079	24.637	255.69	343.40	8.384 2	11.042	7.6982	8.5381	484.58	604.72	423.53	373.93
33.145	1296.500	31.262	31.262	298.16	298.16	9.644 2	9.6442	-	-	-	-	-	-

TABLE 15. Tabulated thermodynamic properties of orthohydrogen at saturation

T (K)	p (kPa)	Liquid ρ (kg/m ³)	Vapor ρ (kg/m ³)	Liquid h (kJ/kg)	Vapor h (kJ/kg)	Liquid s (kJ/kg K)	Vapor s (kJ/kg K)	Liquid c_v (kJ/kg K)	Vapor c_v (kJ/kg K)	Liquid c_p (kJ/kg K)	Vapor c_p (kJ/kg K)	Liquid w (m/s)	Vapor w (m/s)
14.008	7.5600	77.010	0.132 73	-53.820	400.77	-3.062 5	29.390	5.1746	6.2707	7.1448	10.557	1264.7	307.38
15	12.868	76.162	0.212 45	-46.542	409.95	-2.565 4	27.868	5.2658	6.2718	7.4245	10.639	1244.4	316.98
16	20.700	75.280	0.323 28	-38.865	418.79	-2.076 8	26.527	5.3552	6.2935	7.7667	10.775	1224.9	325.79
17	31.665	74.360	0.470 63	-30.794	427.14	-1.596 4	25.341	5.4293	6.3242	8.1490	10.957	1205.4	333.84
18	46.452	73.392	0.660 85	-22.285	434.91	-1.121 6	24.278	5.4920	6.3557	8.5696	11.184	1184.6	341.26
19	65.786	72.371	0.900 72	-13.293	441.99	-0.649 88	23.313	5.5493	6.3859	9.0328	11.465	1162.0	348.11
20	90.417	71.291	1.197 7	-3.769 0	448.30	-0.179 07	22.425	5.6050	6.4172	9.5449	11.813	1137.1	354.41
20.38	101.325	70.864	1.327 2	0.000 32	450.48	1.51E-05	22.104	5.6262	6.4303	9.7541	11.967	1127.0	356.66
21	121.120	70.145	1.560 2	6.339 8	453.74	0.292 85	21.598	5.6609	6.4541	10.115	12.248	1109.8	360.15
22	158.670	68.927	1.997 6	17.094	458.20	0.767 91	20.818	5.7177	6.5019	10.754	12.792	1080.0	365.29
23	203.880	67.627	2.521 2	28.563	461.60	1.248 2	20.076	5.7751	6.5651	11.479	13.478	1047.5	369.78
24	257.550	66.234	3.144 4	40.830	463.80	1.736 0	19.360	5.8333	6.6474	12.315	14.346	1012.3	373.56
25	320.510	64.736	3.884 0	53.994	464.69	2.234 0	18.662	5.8924	6.7514	13.300	15.456	973.92	376.59
26	393.590	63.112	4.761 6	68.184	464.09	2.745 6	17.973	5.9532	6.8795	14.495	16.896	932.22	378.82
27	477.650	61.335	5.806 4	83.575	461.79	3.275 4	17.283	6.0172	7.0338	15.999	18.814	886.71	380.21
28	573.580	59.366	7.059 4	100.41	457.47	3.829 8	16.582	6.0875	7.2168	17.992	21.470	836.74	380.72
29	682.320	57.141	8.583 0	119.08	450.63	4.418 9	15.852	6.1698	7.4321	20.829	25.374	781.37	380.33
30	804.890	54.554	10.481	140.19	440.48	5.060 2	15.070	6.2748	7.6849	25.315	31.669	719.08	378.99
31	942.450	51.390	12.953	164.99	425.43	5.787 8	14.189	6.4265	7.9824	33.767	43.587	647.29	376.59
32	1096.400	47.105	16.504	196.57	401.64	6.690 6	13.099	6.6917	8.3307	56.603	75.154	560.44	373.03
33	1269.000	38.828	23.810	251.54	349.69	8.256 1	11.230	7.4490	8.6394	325.68	406.90	438.23	370.01
33.22	1309.900	31.136	31.136	299.97	299.97	9.682 9	9.6829	-	-	-	-	-	-

The QLCS was used to predict vapor-pressure, near-critical region single-phase density, and speed-of-sound data for normal hydrogen and orthohydrogen. Comparison with existing experimental data for normal hydrogen indicates that the predicted values are within the uncertainty of the existing data sets. The predicted data were used to improve the new normal hydrogen EOS and to create an orthohydrogen EOS.

The estimated uncertainties in the normal hydrogen EOS based on the deviations shown in Figs. 26–37 are similar to those for the new parahydrogen EOS. The deviations in density are as high as 0.1% at temperatures from the triple point to 250 K and at pressures up to 40 MPa, except in the critical region, where an uncertainty of 0.2% in pressure is generally observed. In the region between 250 and 450 K and at pressures up to 300 MPa, the uncertainty in density is 0.04%. At temperatures between 450 and 1000 K, the uncertainty in density increases to 1%. Uncertainties of calculated densities at pressures above 300 MPa increase from 0.04% to a maximum of 1% near the extreme of 2000 MPa. Speed-of-sound data are represented within 0.5% below 100 MPa, except near the critical region. The estimated uncertainty for heat capacities is 1.0%. The estimated uncertainties of vapor pressures and saturated liquid densities calculated using the Maxwell criterion are 0.2% for each property. The increased uncertainty near the critical region versus the new parahydrogen EOS is due to the large deviations among experimental data sets in that region.

The deviations for the orthohydrogen EOS are expected to be similar to those for the formulations of parahydrogen and normal hydrogen, although no comparisons to actual experimental data for orthohydrogen can be made.

The recommendations for future experimental measurements made by Jacobsen *et al.*¹ are emphasized. Recently, a truncated virial equation for use in fuel consumption applications was developed by Lemmon *et al.*⁹⁶ This equation is based on the normal hydrogen EOS developed in this work and provides a correlation for density as a function of temperature and pressure.

There are many applications of hydrogen in mixtures of other fluids including natural gas that may contain greater than 20% hydrogen at various equilibrium states. The equations of state created in this work could be used in a mixture model to accurately determine properties of mixtures of hydrogen with other fluids.

8. Acknowledgments

This paper is dedicated to the life and legacy of Professor Richard B. Stewart (1926–2009), founder and director emeritus of the Center for Applied Thermodynamic Studies at the University of Idaho. Professor Stewart made significant contributions to the early hydrogen literature and to equation of state development. He and his wife, Carol, created the scholarship that partially funded this research.

9. Appendix

Tables 13–15 provide calculated thermodynamic properties at saturation for parahydrogen, normal hydrogen, and orthohydrogen, respectively.

10. References

- R. T. Jacobsen, J. W. Leachman, S. G. Penoncello, and E. W. Lemmon, *Int. J. Thermophys.* **28**, 758 (2007).
- J. W. Leachman, R. T. Jacobsen, S. G. Penoncello, and M. L. Huber, *Int. J. Thermophys.* **28**, 773 (2007).
- J. Leachman, M.S. thesis, University of Idaho, 2007.
- E. W. Lemmon and R. T. Jacobsen, *J. Phys. Chem. Ref. Data* **34**, 69 (2005).
- R. Span, E. W. Lemmon, R. T. Jacobsen, W. Wagner, and A. Yokozeki, *J. Phys. Chem. Ref. Data* **29**, 1361 (2000).
- R. C. Kemp and W. R. Kemp, *Metrologia* **15**, 155 (1979).
- B. A. Younglove, *J. Phys. Chem. Ref. Data* **14**, 619 (1985).
- E. W. Lemmon, M. L. Huber, and M. O. McLinden, *Reference Fluid Thermodynamic and Transport Properties*, NIST Standard Reference Database 23, Version 8.0, National Institute of Standards and Technology, Gaithersburg, MD, 2007.
- K. F. Bonhoeffer and P. Harteck, *Z. Phys. Chem. Abt. B* **4**, 113 (1929).
- A. Eucken and K. Hiller, *Z. Phys. Chem. Abt. B* **4**, 142 (1929).
- W. Heisenberg, *Z. Phys.* **41**, 239 (1927).
- A. Farkas, *Orthohydrogen, Parahydrogen and Heavy Hydrogen* (Cambridge University Press, Cambridge, 1935).
- P. C. Souers, *Hydrogen Properties for Fusion Energy* (University of California Press, Berkeley, 1986).
- J. G. Hust and R. B. Stewart, National Bureau of Standards Report No. 8812, 1965.
- H. W. Woolley, R. B. Scott, and F. G. Brickwedde, National Bureau of Standards Paper No. RP1932, 1948.
- L. Haar, A. S. Friedman, C. W. Beckett, National Bureau of Standards Monograph No. 20, 1961.
- R. Kosloff, R. D. Levine, and R. B. Bernstein, *Mol. Phys.* **27**, 981 (1974).
- R. J. Le Roy, S. G. Chapman, and F. R. W. McCourt, *J. Phys. Chem.* **94**, 923 (1990).
- J. O. Hirschfelder, C. F. Curtiss, and R. B. Bird, *Molecular Theory of Gases and Liquids* (Wiley, New York, 1954).
- J. de Boer, *Physica (Amsterdam)* **14**, 139 (1948).
- J. D. Rogers and F. G. Brickwedde, *J. Chem. Phys.* **42**, 2822 (1965).
- H. F. Knaap and J. J. Beenakker, *Physica (Amsterdam)* **27**, 523 (1961).
- W. van Dael, A. van Itterbeek, A. Cops, and J. Thoen, *Cryogenics* **5**, 207 (1965).
- R. D. McCarty, J. Hord, and H. M. Roder, National Bureau of Standards Monograph No. 168, 1981.
- E. A. Amagat, *Ann. Chim. Phys.* **29**, 68 (1893).
- J. G. Aston, E. Willihnganz, and G. H. Messerly, *J. Am. Chem. Soc.* **57**, 1642 (1935).
- C. R. Barber, in *Comité International des Poids et Mesures. Comité Consultatif de Thermométrie* (Gauthier, Paris, 1964), p. 94.
- C. R. Barber and A. Horsford, *Br. J. Appl. Phys.* **14**, 920 (1963).
- E. P. Bartlett, *J. Am. Chem. Soc.* **49**, 687 (1927).
- E. P. Bartlett, H. L. Cupples, and T. H. Tremearne, *J. Am. Chem. Soc.* **50**, 1275 (1928).
- E. P. Bartlett, H. C. Hetherington, H. M. Kvalnes, and T. H. Tremearne, *J. Am. Chem. Soc.* **52**, 1363 (1930).
- J. J. M. Beenakker, F. H. Varekamp, and A. van Itterbeek, *Commun. Kamerlingh Onnes Lab. Univ. Leiden, Suppl.* **313A**, 1 (1959).
- T. W. Bradshaw and J. O. W. Norris, *Rev. Sci. Instrum.* **58**, 83 (1987).
- J. P. Brouwer, C. J. N. van den Meijdenberg, and J. J. M. Beenakker, *Commun. Kamerlingh Onnes Lab. Univ. Leiden, Suppl.* **380a**, 1 (1970).
- T. L. Cottrell, R. A. Hamilton, and R. P. Taubinger, *Trans. Faraday Soc.* **52**, 1310 (1956).
- H. G. David and S. D. Hamann, *Trans. Faraday Soc.* **49**, 711 (1953).
- W. J. Dehaas, *Proc. K. Ned. Akad. Wet.* **15**, 295 (1912).
- Z. E. H. A. El Hadi, J. A. Dorrepaal, and M. Durieux, *Physica (Amsterdam)* **41**, 320 (1969).

- ³⁹ C. W. Gibby, C. C. Tanner, and I. Masson, *Proc. R. Soc. London* **122**, 283 (1929).
- ⁴⁰ R. D. Goodwin, D. E. Diller, H. M. Roder, and L. A. Weber, *J. Res. Natl. Bur. Stand.* **68**, 121 (1964).
- ⁴¹ R. D. Goodwin, D. E. Diller, H. M. Roder, and L. A. Weber, *J. Res. Natl. Bur. Stand.* **67**, 173 (1963).
- ⁴² R. D. Goodwin, D. E. Diller, H. M. Roder, and L. A. Weber, *Cryogenics* **2**, 81 (1961).
- ⁴³ E. R. Grilly, *J. Am. Chem. Soc.* **73**, 843 (1951).
- ⁴⁴ D. Güsewell, F. Schmeissner, and J. Schmid, *Cryogenics* **10**, 150 (1970).
- ⁴⁵ F. Henning, *Z. Phys.* **40**, 775 (1927).
- ⁴⁶ F. Henning and J. Otto, *Phys. Z.* **37**, 633 (1936).
- ⁴⁷ M. J. Hiza, *Fluid Phase Equilib.* **6**, 203 (1981).
- ⁴⁸ H. J. Hoge and R. D. Arnold, *J. Res. Natl. Bur. Stand.* **47**, 63 (1951).
- ⁴⁹ H. J. Hoge and J. W. Lassiter, *J. Res. Natl. Bur. Stand.* **47**, 75 (1951).
- ⁵⁰ L. Holborn and J. Otto, *Z. Phys.* **38**, 359 (1926).
- ⁵¹ L. Holborn and J. Otto, *Z. Phys.* **33**, 1 (1925).
- ⁵² M. Jaeschke and A. E. Humphreys, *The GERG Databank of High Accuracy Compressibility Factor Measurements GERG Technical Monograph 4* (Verlag des Vereins Deutscher Ingenieure, Düsseldorf, Germany, 1990).
- ⁵³ H. L. Johnston, J. T. Clarke, E. B. Rifkin, and E. C. Kerr, *J. Am. Chem. Soc.* **72**, 3933 (1950).
- ⁵⁴ H. L. Johnston, W. E. Keller, and A. S. Friedman, *J. Am. Chem. Soc.* **76**, 1482 (1954).
- ⁵⁵ H. L. Johnston, D. White, H. Wirth, C. Swanson, L. H. Jensen, and A. S. Friedman, Cryogenic Laboratory, Ohio State University Report No. 264-25, 1953.
- ⁵⁶ W. H. Keesom, A. Bijl, and H. van der Horst, *Commun. Kamerlingh Onnes Lab. Univ. Leiden, Suppl.* **214A**, 1 (1931).
- ⁵⁷ K. Kerl, *Z. Phys. Chem.* **129**, 129 (1982).
- ⁵⁸ H. F. P. Knaap, M. Knoester, C. M. Knobler, and J. J. M. Beenakker, *Commun. Kamerlingh Onnes Lab. Univ. Leiden, Suppl.* **330C**, 1 (1962).
- ⁵⁹ D. H. Liebenberg, R. L. Mills, and J. C. Bronson, *Phys. Rev. B* **18**, 4526 (1978).
- ⁶⁰ D. H. Liebenberg, R. L. Mills, and J. C. Bronson, Los Alamos National Laboratory Report No. LA-6641-MS, 1977.
- ⁶¹ E. A. Long and O. L. I. Brown, *J. Am. Chem. Soc.* **59**, 1922 (1937).
- ⁶² E. S. Lopatinskii, M. S. Rozhnov, V. I. Zhdanov, S. L. Pernovskii, and Y. N. Kudrya, *Zh. Fiz. Khim.* **65**, 2060 (1991).
- ⁶³ J. R. S. Machado, W. B. Streett, and U. Deiters, *J. Chem. Eng. Data* **33**, 148 (1988).
- ⁶⁴ V. A. Medvedev, Yu. A. Dedikov, and M. P. Orlova, *Russ. J. Phys. Chem.* **45**, 297 (1971).
- ⁶⁵ A. Michels, W. De Graaff, T. Wassenaar, J. M. H. Levelt, and P. Louw-erse, *Physica (Amsterdam)* **25**, 25 (1959).
- ⁶⁶ A. Michels, W. De Graaf, and C. A. Ten Seldam, *Physica (Amsterdam)* **26**, 393 (1960).
- ⁶⁷ A. Michels and M. Goudekot, *Physica (Amsterdam)* **8**, 353 (1941).
- ⁶⁸ S. Mihara, H. Sagara, Y. Arai, and S. Saito, *J. Chem. Eng. Jpn.* **10**, 395 (1977).
- ⁶⁹ W. H. Mueller, T. W. Leland, and R. Kobayashi, *AIChE J.* **7**, 267 (1961).
- ⁷⁰ G. P. Nijhoff and W. H. Keesom, *Commun. Kamerlingh Onnes Lab. Univ. Leiden, Suppl.* **188D**, 31 (1927).
- ⁷¹ S. Perez, H. Schmiedel, and B. Schramm, *Z. Phys. Chem.* **123**, 35 (1980).
- ⁷² D. C. Presnall, *J. Geophys. Res.* **74**, 6026 (1969).
- ⁷³ H. M. Roder, D. E. Diller, L. A. Weber, and R. D. Goodwin, *Cryogenics* **3**, 16 (1963).
- ⁷⁴ G. E. Schmauch and A. H. Singleton, *Ind. Eng. Chem.* **56**, 20 (1964).
- ⁷⁵ B. Schramm, E. Elias, L. Kern, Gh. Natour, A. Schmitt, and Ch. Weber, *Ber. Bunsenges. Phys. Chem.* **95**, 615 (1991).
- ⁷⁶ G. A. Scott, *Proc. R. Soc. London, Ser. A* **125**, 330 (1929).
- ⁷⁷ R. B. Scott, F. G. Brickwedde, H. C. Urey, and M. H. Wahl, *J. Chem. Phys.* **2**, 454 (1934).
- ⁷⁸ U. Setzmann and W. Wagner, *J. Phys. Chem. Ref. Data* **20**, 1061 (1991).
- ⁷⁹ A. L. Smith, N. C. Hallett, and H. L. Johnston, *J. Am. Chem. Soc.* **76**, 1486 (1954).
- ⁸⁰ D. T. A. Townend and L. A. Bhatt, *Proc. R. Soc. London, Ser. A* **134**, 502 (1931).
- ⁸¹ M. W. Travers, G. Senter, and A. Jaquerod, *Proc. R. Soc. London* **70**, 484 (1902).
- ⁸² F. P. G. A. J. van Agt and H. Kamerlingh Onnes, Redstone Science Information Center Translation No. RSIC-30, 1963.
- ⁸³ A. van Itterbeek, W. van Dael, and A. Cops, *Physica (Amsterdam)* **29**, 965 (1963).
- ⁸⁴ A. van Itterbeek, W. van Dael, and A. Cops, *Physica (Amsterdam)* **27**, 111 (1961).
- ⁸⁵ A. van Itterbeek, O. Verbeke, F. Theeuwes, and V. Janssone, *Physica (Amsterdam)* **32**, 1591 (1966).
- ⁸⁶ A. van Itterbeek, O. Verbeke, F. Theeuwes, K. Staes, and J. de Boelpaep, *Physica (Amsterdam)* **30**, 1238 (1964).
- ⁸⁷ F. H. Verekamp and J. J. M. Beenakker, *Commun. Kamerlingh Onnes Lab. Univ. Leiden, Suppl.* **316C**, 1 (1959).
- ⁸⁸ T. T. H. Verschoyle, *Proc. R. Soc. London* **A111**, 552 (1926).
- ⁸⁹ L. A. Weber, D. E. Diller, H. M. Roder, and R. D. Goodwin, *Cryogenics* **2**, 236 (1962).
- ⁹⁰ D. White, A. S. Friedman, and H. L. Johnston, *J. Am. Chem. Soc.* **72**, 3565 (1950).
- ⁹¹ D. White, A. S. Friedman, and H. L. Johnston, *J. Am. Chem. Soc.* **72**, 3927 (1950).
- ⁹² R. Wiebe and V. L. Gaddy, *J. Am. Chem. Soc.* **60**, 2300 (1938).
- ⁹³ B. A. Younglove, *J. Acoust. Soc. Am.* **38**, 433 (1965).
- ⁹⁴ B. A. Younglove and D. E. Diller, *Cryogenics* **2**, 348 (1962).
- ⁹⁵ B. A. Younglove and D. E. Diller, *Cryogenics* **2**, 283 (1962).
- ⁹⁶ E. W. Lemmon, M. L. Huber, and J. W. Leachman, *J. Res. Natl. Inst. Stand. Technol.* **113**, 341 (2008).